Mon. Not. R. Astron. Soc. **000**, 000–000 (1997) Printed 2 October 2002

Stability of Power-Law Disks I – The Fredholm Integral Equation

N. W. Evans and J. C. A. Read
Theoretical Physics, Department of Physics, 1 Keble Rd, Oxford, OX1 3NP

2 October 2002

ABSTRACT

The power-law disks are a family of infinitesimally thin, axisymmetric stellar disks of infinite extent. The rotation curve can be rising, falling or flat. The self-consistent power-law disks are scale-free, so that all physical quantities vary as a power of radius. They possess simple equilibrium distribution functions depending on the two classical integrals, energy and angular momentum. While maintaining the scale-free equilibrium force law, the power-law disks can be transformed into cut-out disks by preventing stars close to the origin (and sometimes also at large radii) from participating in any disturbance.

This paper derives the homogeneous Fredholm integral equation for the in-plane normal modes in the self-consistent and the cut-out power-law disks. This is done by linearising the collisionless Boltzmann equation to find the response density corresponding to any imposed density and potential. The normal modes – that is, the self-consistent modes of oscillation – are found by requiring the imposed density to equal the response density. In practice, this scheme is implemented in Fourier space, by decomposing both imposed and response densities in logarithmic spirals. The Fredholm integral equation then relates the transform of the imposed density to the transform of the response density. Numerical strategies to solve the integral equation and to isolate the growth rates and the pattern speeds of the normal modes are discussed.

Key words: celestial mechanics, stellar dynamics – galaxies: kinematics and dynamics – galaxies: spiral – methods: analytical – methods: numerical

1 INTRODUCTION

This paper begins an investigation into the large-scale, global, linear modes of a family of horizontally hot, vertically cold, idealised disk galaxies with rising, falling or flat rotation curves. Here, we collect all the mathematical and numerical details needed for our study. A companion paper completes the investigation by presenting results on the global spiral modes, together with the astrophysical implications. The focus is exclusively on the in-plane instabilities, such as the modes causing bar-like or lop-sided distortions. Of course, our hot, razor-thin models are also unstable to bending modes (Merritt & Sellwood 1994). These are ignored because they almost certainly can be eliminated by giving the disks a modest thickness.

In our study, we have the good fortune to be able to follow a magisterial earlier analysis carried out by Zang (1976). This remarkable Ph. D. thesis was supervised by Alar Toomre and also benefited from a number of ingenious suggestions provided by Agris Kalnajs. What Zang did in the mid-seventies was to carry out the first complete, global, stability analysis for a family of differentially rotating, stellar dynamical disks. The object of his study was an infinitesimally thin disk in which the circular velocity is completely flat. The special case in which the stars move on circular orbits is known as the Mestel (1963) disk. Their hot stellar dynamical counterparts are usually called the Toomre-Zang disks. The global spiral modes in this model were described extensively by Zang.

The power-law disks are infinitesimally thin disks in which the circular velocity varies as a power of cylindrical polar radius, viz., $v_{\rm circ} \propto R^{-\beta/2}$. They are amongst the simplest stellar dynamical disks known – the distributions of stellar velocities that build the models are given by Evans (1994). Their rotation curves can be rising or falling. The self-similarity of these disks simplifies the analysis considerably. It enables much of the global normal mode

calculation to be performed exactly. The model examined in Zang's (1976) thesis is the particular case with a completely flat rotation curve ($\beta = 0$). The perfectly self-similar disks are somewhat special. To supplement our analysis, we have also concentrated on a modified version of the pure power-law disks, in which the central regions of the disks are immobilised or cut-out. This was achieved by reducing the fraction of active stars – those able to respond to any disturbance – from unity at moderate radii to zero at the centre. In order to aid comparison of our results with numerical simulations, especially those of Earn (1993), we have also tapered the fraction of active stars to zero at large radii. The immobile components still contribute to the potential experienced by the stars. The material in Zang's (1976) thesis was never completely published, although some of these and various subsequent calculations are reported in Toomre (1977; 1981). So, we urge the reader to remember that our contribution consists *only* in generalising the analysis of Zang from the disk with a completely flat rotation curve to the entire family of power-law disks. This is not trivial, as the limit of a flat rotation curve is a singular one. Nonetheless, our job has been very considerably eased by being able to lean on the sturdy support of Zang and his two implicit co-workers. We use the notation Z followed by an equation number as a convenient shorthand for reference to Zang's (1976) thesis.

The aim of this paper is to derive the homogeneous, singular, Fredholm integral equation for the normal modes in the self-consistent and the cut-out power-law disks. First, the equilibrium properties of the models are introduced in Section 2. The collisionless Boltzmann equation is linearised to derive the Fredholm integral equation in Section 3. Section 4 summarises the strategies for its computational solution. This paper describes only methods. The following paper in this issue of *Monthly Notices* presents the numerical results and astrophysical consequences.

2 THE EQUILIBRIUM DISKS

This section begins with a brief introduction to the power-law disks. Section 2.2 introduces new variables – the home radius and the eccentric velocity – which can be used to characterise the stellar orbits according to their size and shape. The frequencies and the periods of orbits are derived in the next section. The equilibrium distribution functions of stellar velocities of the self-consistent power-law disks are presented in Section 2.4. The concluding section explains how to "cut out" the centre of the disk and to taper the disk at large radii. Both these require changes to the distribution function.

2.1 The Potential-Density Pair

The equilibrium density of the power-law disks is

$$\Sigma_{\rm eq} = \Sigma_0 \left(\frac{R_0}{R}\right)^{1+\beta}. \tag{1}$$

The self-consistent potential in the plane of the disk is (Schmitz & Ebert 1987; Lemos *et al.* 1991; Evans 1994)

$$\psi(R) = \frac{v_\beta^2}{\beta}\left(\frac{R_0}{R}\right)^{\beta}, \tag{2}$$

where the reference velocity v_β is defined as

$$v_\beta^2 = 2\pi G\Sigma_0 R_0 \frac{\Gamma\left[\frac{1}{2}(1-\beta)\right]\Gamma\left[\frac{1}{2}(2+\beta)\right]}{\Gamma\left[\frac{1}{2}(1+\beta)\right]\Gamma\left[\frac{1}{2}(2-\beta)\right]}. \tag{3}$$

Clearly (2) fails for $\beta = 0$. In this case, we have (Mestel 1963)

$$\psi(R) = -v_0^2 \ln\left(\frac{R}{R_0}\right). \tag{4}$$

Whenever an expression fails at $\beta = 0$, the corresponding result for the Toomre-Zang disk should be used. It can often be derived by taking the limit $\beta \to 0$ with l'Hôpital's theorem. The circular velocity is

$$v_{\rm circ}^2 = \left(\frac{R_0}{R}\right)^{\beta} v_\beta^2. \tag{5}$$

Thus, the reference velocity v_β is the circular velocity at the reference radius R_0. Disks with $\beta > 0$ have falling rotation curves, whereas disks with $\beta < 0$ have rising rotation curves. Disk galaxies typically have flattish rotation

curves (e.g. Rubin *et al.* 1978; Mihalas & Binney 1987) – sometimes slowly rising, sometimes slowly falling at large radii (Casertano & van Gorkom 1991). The total mass of the disk is infinite for all β in the range $-1 \leq \beta < 1$. The mass enclosed within a radius R is

$$M(R) = \frac{2\pi\Sigma_0 R_0^2}{1-\beta}\left(\frac{R}{R_0}\right)^{1-\beta}. \tag{6}$$

2.2 The Home Radius and the Eccentric Velocity

The Lagrangian for stars orbiting in a general power-law disk is

$$\mathcal{L} = \frac{1}{2}\dot{R}^2 + \frac{1}{2}R^2\dot{\theta}^2 + \frac{v_\beta^2}{\beta}\left(\frac{R_0}{R}\right)^\beta. \tag{7}$$

There are two isolating integrals of motion, namely the energy E and the angular momentum L_z. In terms of the radial velocity $u = \dot{R}$ and the tangential velocity $v = R\dot{\theta}$, the integrals are

$$L_z = Rv, \qquad\qquad E = \frac{1}{2}\left(u^2+v^2\right) - \frac{v_\beta^2}{\beta}\left(\frac{R_0}{R}\right)^\beta. \tag{8}$$

Following Zang (1976), let us define the *home radius* $R_{\rm H}$ to be the radius at which the tangential velocity is equal to the circular velocity. By conservation of angular momentum, we have

$$R_{\rm H} = R_0\left(\frac{L_z}{v_\beta R_0}\right)^{\frac{2}{2-\beta}}. \tag{9}$$

Again following Zang (1976), the *eccentric velocity* U is defined as the maximum radial speed reached during an orbit. U is thus positive by definition. It is easy to show that the eccentric velocity is attained at the home radius (9) and that its value is given by

$$U^2 = 2E + \left(\frac{2}{\beta}-1\right)\left(\frac{v_\beta^2 R_0^\beta}{L_z^\beta}\right)^{\frac{2}{2-\beta}}. \tag{10}$$

A similar derivation using the potential of the Mestel disk gives the result already well-known to Zang (Z2.29)

$$U^2 = 2E - v_0^2\left(1 + 2\ln\frac{L_z}{v_0 R_0}\right). \tag{11}$$

We shall find it convenient to work in dimensionless co-ordinates. We define the following dimensionless integrals of motion:

$$\tilde{U}^2 = \frac{U^2}{v_\beta^2}\left(\frac{R_{\rm H}}{R_0}\right)^\beta, \qquad \tilde{R}_{\rm H} = \frac{R_{\rm H}}{R_0}, \qquad \tilde{E} = \frac{E}{v_\beta^2}\left(\frac{R_{\rm H}}{R_0}\right)^\beta, \qquad \tilde{L}_z = \frac{L_z}{v_\beta R_0}. \tag{12}$$

Likewise, dimensionless radial and tangential velocities, radius and time coordinates can be defined as:

$$\tilde{u}^2 = \frac{u^2}{v_\beta^2}\left(\frac{R_{\rm H}}{R_0}\right)^\beta, \qquad \tilde{v}^2 = \frac{v^2}{v_\beta^2}\left(\frac{R_{\rm H}}{R_0}\right)^\beta, \qquad \tilde{R} = \frac{R}{R_{\rm H}}, \qquad \tilde{t} = \frac{v_\beta}{R_{\rm H}}\left(\frac{R_0}{R_{\rm H}}\right)^{\beta/2} t. \tag{13}$$

The scaled energy (8), home radius (9) and eccentric velocity (10) are given by

$$\tilde{E} = \frac{1}{2}\left(\tilde{u}^2+\tilde{v}^2\right) - \frac{1}{\beta\tilde{R}^\beta}, \qquad \tilde{R}_{\rm H} = \tilde{L}_z^{\frac{2}{2-\beta}}, \qquad \tilde{U}^2 = 2\tilde{E} - 1 + \frac{2}{\beta}. \tag{14}$$

We will also need expressions for the scaled radial and tangential velocities:

$$\tilde{u}^2 = \tilde{U}^2 + 1 - \tilde{R}^{-2} + \frac{2}{\beta}\left(\tilde{R}^{-\beta} - 1\right), \qquad \tilde{v} = \frac{1}{\tilde{R}}. \tag{15}$$

In terms of the scaled coordinates, the equations of motion derived from the Lagrangian become

$$\frac{d^2\tilde{R}}{d\tilde{t}^2} = \frac{1}{\tilde{R}^3} - \frac{1}{\tilde{R}^{1+\beta}}, \qquad \frac{d\theta}{d\tilde{t}} = \frac{1}{\tilde{R}^2}. \tag{16}$$

Imagine solving the equations of motions with starting positions and velocities. If two stars have the same $\tilde{u}$ and $\tilde{v}$, then their orbits have the same shape, although the size of the orbit is proportional to $R_{\rm H}$. This leads us to an intuitive understanding of the eccentric velocity and the home radius. Stellar orbits with the same dimensionless eccentric velocity have the same shape. The dimensionless home radius fixes the overall size of the orbit.

The star's orbit in the equilibrium disk is limited by its isolating integrals of motion. In terms of the dimensionless co-ordinates, the turning-points of the orbit occur when

$$\tilde{u}^2 = \tilde{U}^2 + 1 - \tilde{R}^{-2} + \frac{2}{\beta}\left(\tilde{R}^{-\beta} - 1\right) = 0. \tag{17}$$

For given $\tilde{U}$ and β, there are two solutions, $\tilde{R}_{\rm min}$ corresponding to pericentre, and $\tilde{R}_{\rm max}$ corresponding to apocentre. These are easy to find numerically by the Newton-Raphson technique. The star thus moves within an annulus of the disk. For certain values of the eccentric velocity, the orbit closes, and the star then traverses a one-dimensional manifold within the annulus; in general, the orbit does not close, and the star eventually passes arbitrarily close to every region of the annulus.

2.3 Periods and Frequencies

Let us start by defining a useful auxiliary integral

$$\mathcal{J}_n(\tilde{U}) = 2\int_{\tilde{R}_{\rm min}(\tilde{U})}^{\tilde{R}_{\rm max}(\tilde{U})} \frac{d\tilde{R}}{\tilde{R}^n\left(\tilde{U}^2 + 1 - \tilde{R}^{-2} + \frac{2}{\beta}\left(\tilde{R}^{-\beta} - 1\right)\right)^{\frac{1}{2}}}, \tag{18}$$

where $\tilde{R}_{\rm min}$ and $\tilde{R}_{\rm max}$ are the solutions of (17). For the $\beta = 0$ case, this becomes (Z2.39)

$$\mathcal{J}_n(\tilde{U}) = 2\int_{\tilde{R}_{\rm min}(\tilde{U})}^{\tilde{R}_{\rm max}(\tilde{U})} \frac{d\tilde{R}}{\tilde{R}^n\left(\tilde{U}^2 + 1 - \tilde{R}^{-2} - 2\ln\tilde{R}\right)^{\frac{1}{2}}}. \tag{19}$$

To evaluate $\mathcal{J}_n$ numerically, we remove the singularities at either end of the integrand by transforming to a variable θ. We define $\tilde{R} = m + a\sin\theta$, where m is the midpoint of the radial motion, $m = \frac{1}{2}(\tilde{R}_{\rm min} + \tilde{R}_{\rm max})$ and a is its amplitude, $a = \frac{1}{2}(\tilde{R}_{\rm min} - \tilde{R}_{\rm max})$. The integration can then be carried out using the midpoint method (Press *et al.* 1989, chap. 4).

The radial period T is the time taken for the star to travel between two successive pericentres: i.e., to move out and in again. The corresponding radial frequency is defined by $\kappa = 2\pi/T$. Using the symmetry of the orbit, we have

$$T = 2\int_{R=R_{\rm min}}^{R=R_{\rm max}} dt = 2\int_{R_{\rm min}}^{R_{\rm max}} \frac{dR}{\dot{R}} = \frac{2R_{\rm H}}{v_\beta}\left(\frac{R_{\rm H}}{R_0}\right)^{\frac{\beta}{2}} \int_{\tilde{R}_{\rm min}}^{\tilde{R}_{\rm max}} \frac{d\tilde{R}}{\tilde{u}}. \tag{20}$$

Using the expression for the radial velocity given in (15), along with the definition (18), we find that the radial period and frequency are

$$T = \frac{R_{\rm H}}{v_\beta}\left(\frac{R_{\rm H}}{R_0}\right)^{\frac{\beta}{2}} \mathcal{J}_0, \qquad \kappa = \frac{2\pi}{T} = \frac{v_\beta}{R_{\rm H}}\left(\frac{R_0}{R_{\rm H}}\right)^{\frac{\beta}{2}} \frac{2\pi}{\mathcal{J}_0}. \tag{21}$$

We shall find it useful to define the dimensionless radial frequency $\tilde{\kappa}$:

$$\tilde{\kappa} = \frac{R_{\rm H}}{v_\beta}\left(\frac{R_{\rm H}}{R_0}\right)^{\frac{\beta}{2}} \kappa = \frac{2\pi}{\mathcal{J}_0}. \tag{22}$$

The angular period Θ is defined to be the angle through which a star moves during the time taken to complete one radial oscillation:

$$\Theta = \int_{t=0}^{t=T} d\theta = 2\int_{R_{\rm min}}^{R_{\rm max}} \frac{\dot{\theta}}{\dot{R}} dR = 2\int_{R_{\rm min}}^{R_{\rm max}} \frac{v dR}{uR} = 2\int_{\tilde{R}_{\rm min}}^{\tilde{R}_{\rm max}} \frac{\tilde{v} d\tilde{R}}{\tilde{u}\tilde{R}} = \mathcal{J}_2. \tag{23}$$

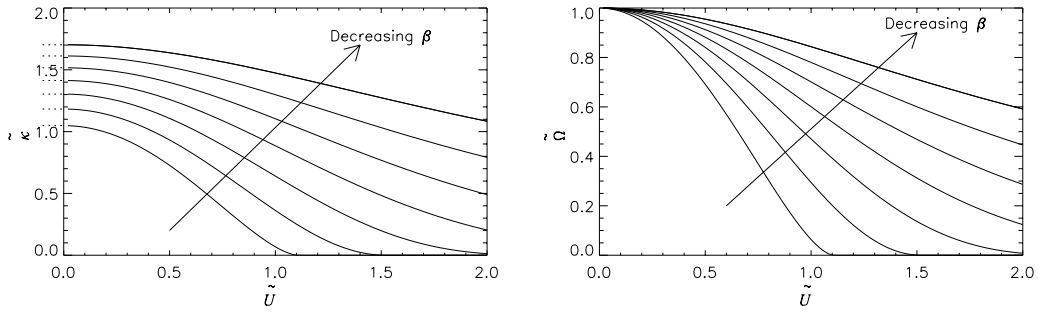

Figure 1. The radial frequency $\tilde{\kappa}$ and angular frequency $\tilde{\Omega}$ plotted against eccentric velocity $\tilde{U}$, for β = -0.9, -0.6, -0.3, 0, +0.3, +0.6, +0.9. In the left-hand plot, the dotted lines on the vertical axis mark the epicyclic limit of $\sqrt{2-\beta}$. As $\tilde{U} \to \infty$, the frequencies $\tilde{\kappa}$ and $\tilde{\Omega}$ remain positive but become vanishingly small.

The angular frequency Ω is defined to be the mean angular speed of the star: $\Omega = \Theta/T$. We shall commonly use the dimensionless angular frequency $\tilde{\Omega}$, where

$$\tilde{\Omega} = \frac{R_{\rm H}}{v_\beta}\left(\frac{R_{\rm H}}{R_0}\right)^{\frac{\beta}{2}}\Omega = \frac{\mathcal{J}_2}{\mathcal{J}_0}. \tag{24}$$

The dependence of $\tilde{\kappa}$ and $\tilde{\Omega}$ on $\tilde{U}$ and β is shown in Fig. 1. In the limit $\tilde{U} \to 0$, the dimensionless epicyclic and circular frequencies are

$$\tilde{\kappa}_0 \equiv \lim_{\tilde{U}\to 0}\tilde{\kappa} = \sqrt{2-\beta}, \qquad\qquad \tilde{\Omega}_0 \equiv \lim_{\tilde{U}\to 0}\tilde{\Omega} = 1. \tag{25}$$

In the limit $\tilde{U} \to \infty$, these frequencies tend to zero from above. As expected, the angular frequency is that of a star in a circular orbit at $R_{\rm H}$, namely $\Omega_0 = v_{\rm circ}/R_{\rm H}$. At low eccentric velocity, there is superimposed on this circular motion a small radial oscillation with frequency $\kappa_0 = \sqrt{2-\beta}\,v_{\rm circ}/R_{\rm H}$. This is of course just the epicyclic approximation for near-circular orbits (Binney & Tremaine 1987).

2.4 The Structure of Phase Space

The distribution function of the stars can depend on positions and velocities only through the isolating integrals of motion, according to Jeans' (1919) theorem. Even quite simple disks can possess rather complicated distribution functions (Evans & Collett 1993). The power-law disks are attractive candidates for a stability analysis because they possess a rich family of simple self-consistent distribution functions $f_{\rm s}$ found by Evans (1994). These are built from powers of energy and angular momentum, and normalised so that the integral of the distribution function over all velocities recovers the surface density. They are:

$$f_{\rm s}(E, L_z) = \tilde{C} L_z^\gamma |E|^{1/\beta+\gamma/\beta-\gamma/2}, \qquad \text{where} \qquad \tilde{C} = \frac{C_{\beta\gamma}\Sigma_0|\beta|^{1+\frac{1}{\beta}+\frac{\gamma}{\beta}}}{2^{\gamma/2}\sqrt{\pi}R_0^\gamma v_\beta^{2\left(1+\frac{1}{\beta}+\frac{\gamma}{\beta}\right)}}; \tag{26}$$

with

$$\beta > 0: \qquad C_{\beta\gamma} = \frac{\Gamma\left[2+\frac{1}{\beta}+\frac{\gamma}{\beta}\right]}{\Gamma\left[\frac{1}{2}(\gamma+1)\right]\Gamma\left[1+\frac{1}{\beta}+\frac{\gamma}{\beta}-\frac{\gamma}{2}\right]}, \qquad \text{and} \qquad \gamma > -1; \tag{27}$$

$$\beta < 0: \qquad C_{\beta\gamma} = \frac{\Gamma\left[\frac{\gamma}{2}-\frac{1}{\beta}-\frac{\gamma}{\beta}\right]}{\Gamma\left[\frac{1}{2}(\gamma+1)\right]\Gamma\left[-1-\frac{1}{\beta}-\frac{\gamma}{\beta}\right]}, \qquad \text{and} \qquad \gamma > -\beta-1. \tag{28}$$

Note that these formulae differ by a factor of two from those given in Evans' (1994) paper. This is because Evans' results assume a bi-directional disk, where the stars rotate in both senses. In this paper, we consider only uni-directional

disks. Analogous distribution functions for the Toomre-Zang disk have been known for a long time (Bisnovatyi-Kogan 1976; Zang 1976; Toomre 1977; Binney & Tremaine 1987, chap. 4)

$$f_{\rm s}(E,L_z) = \tilde{C} L_z^{\gamma} \exp\left(-(\gamma+1)\frac{E}{v_0^2}\right), \qquad \text{where } \tilde{C} = \frac{C_{0\gamma}\Sigma_0}{2^{\gamma/2}\sqrt{\pi}R_0^{\gamma}v_0^{\gamma+2}}, \qquad C_{0\gamma} = \frac{(\gamma+1)^{1+\gamma/2}}{\Gamma\left[\frac{1}{2}(\gamma+1)\right]}. \tag{29}$$

In these formulae, γ is a constant anisotropy parameter. Its physical meaning will shortly become apparent on examining the dynamical quantities derived from the distribution function.

The mean streaming velocity, or the stellar rotation curve, is

$$\langle v\rangle = v_\beta\sqrt{\frac{2}{\beta}}\frac{\Gamma\left[1+\frac{\gamma}{2}\right]}{\Gamma\left[\frac{1}{2}+\frac{\gamma}{2}\right]}\frac{\Gamma\left[2+\frac{1}{\beta}+\frac{\gamma}{\beta}\right]}{\Gamma\left[\frac{5}{2}+\frac{1}{\beta}+\frac{\gamma}{\beta}\right]}\left(\frac{R_0}{R}\right)^{\beta/2}, \qquad \beta>0, \tag{30}$$

$$\langle v\rangle = v_\beta\sqrt{\frac{2}{-\beta}}\frac{\Gamma\left[1+\frac{\gamma}{2}\right]\Gamma\left[-\frac{3}{2}-\frac{1}{\beta}-\frac{\gamma}{\beta}\right]}{\Gamma\left[\frac{1}{2}+\frac{\gamma}{2}\right]\Gamma\left[-1-\frac{1}{\beta}-\frac{\gamma}{\beta}\right]}\left(\frac{R}{R_0}\right)^{-\beta/2}, \qquad \beta<0, \tag{31}$$

$$\langle v\rangle = v_0\sqrt{\frac{2}{1+\gamma}}\frac{\Gamma\left[1+\frac{\gamma}{2}\right]}{\Gamma\left[\frac{1}{2}+\frac{\gamma}{2}\right]}, \qquad \beta=0. \tag{32}$$

The radial velocity dispersion σ_u is the root-mean-squared radial velocity of the stars. We shall also find it convenient to define a dimensionless radial velocity dispersion $\tilde{\sigma}_u$. These are:

$$\sigma_u^2 = \frac{v_\beta^2}{1+\gamma+2\beta}\left(\frac{R_0}{R}\right)^{\beta}, \qquad \tilde{\sigma}_u^2 = \left(\frac{R}{R_0}\right)^{\beta}\frac{\sigma_u^2}{v_\beta^2} = \frac{1}{1+\gamma+2\beta}. \tag{33}$$

If all the stars move on circular orbits, the radial velocity dispersion vanishes. Such a disk is said to be "cold", by analogy with the motion of molecules in gases. As the eccentricity of the orbits increases, the stars acquire random motions and thus the "temperature" of the disk increases. High values of the anisotropy parameter γ correspond to low velocity dispersions, i.e., cold disks. This is obvious on examining the form of the distribution function: $f_{\rm s} \propto L_z^{\gamma}$. When γ is large, more of the stars have high angular momentum and lie on near-circular orbits. The isotropic model is given by $\gamma = 0$. The squared tangential velocity dispersion σ_v^2 is the difference between the second tangential velocity moment $\langle v^2\rangle$ and the square of the mean streaming velocity $\langle v\rangle^2$. The second moment $\langle v^2\rangle$ is derived from the distribution function as:

$$\langle v^2\rangle = \frac{v_\beta^2(1+\gamma)}{1+\gamma+2\beta}\left(\frac{R_0}{R}\right)^{\beta} = (1+\gamma)\sigma_u^2. \tag{34}$$

As $\gamma\to\infty$, $\sigma_u^2\to 0$ and $\sqrt{\langle v^2\rangle}\to v_{\rm circ}$, so the disk is rotationally supported. These distribution functions have the property that, at any spot, the ratio of radial velocity dispersion to mean squared tangential velocity is constant.

It has been conjectured (Ostriker & Peebles 1973) that the global stability of disks is related to the ratio of the total rotational energy to the total potential energy. As part of our aim is to examine this claim, let us derive the global virial quantities for future reference. The total kinetic energy $K(R)$ and potential energy $W(R)$ within any radius R can be computed as

$$K(R) = \pi\Sigma_0 v_\beta^2 R_0^2\frac{2+\gamma}{(1+\gamma+2\beta)(1-2\beta)}\left(\frac{R}{R_0}\right)^{1-2\beta}, \qquad W(R) = -\frac{2\pi\Sigma_0 v_\beta^2 R_0^2}{1-2\beta}\left(\frac{R}{R_0}\right)^{1-2\beta}. \tag{35}$$

For the power-law disks, the virial theorem takes the form

$$2K(R) + \frac{2+\gamma}{1+\gamma+2\beta}W(R) = 0. \tag{36}$$

Note that the power-law disks do not, in general, satisfy the standard virial theorem $2K+W=0$. This is because it is not possible to "enclose" the system with a sufficiently large container. No matter how large the container, if the disk is warm, some stars will always cross its surface. When the disk is perfectly cold, the stars have no radial

motion and thus do not cross the surface. In this case, as seen from eq. (36), the standard virial theorem does hold. (Similar comments hold good for the isothemal sphere, for example). The rotational kinetic energy is

$$T(R) = \frac{2\pi\Sigma_0 v_\beta^2 R_0^2}{\beta(1-2\beta)} \frac{\Gamma^2\left[1+\frac{\gamma}{2}\right]\Gamma^2\left[2+\frac{1}{\beta}+\frac{\gamma}{\beta}\right]}{\Gamma^2\left[\frac{1}{2}+\frac{\gamma}{2}\right]\Gamma^2\left[\frac{5}{2}+\frac{1}{\beta}+\frac{\gamma}{\beta}\right]} \left(\frac{R}{R_0}\right)^{1-2\beta}, \qquad \beta > 0, \tag{37}$$

$$T(R) = -\frac{2\pi\Sigma_0 v_\beta^2 R_0^2}{\beta(1-2\beta)} \frac{\Gamma^2\left[1+\frac{\gamma}{2}\right]\Gamma^2\left[-\frac{3}{2}-\frac{1}{\beta}-\frac{\gamma}{\beta}\right]}{\Gamma^2\left[\frac{1}{2}+\frac{\gamma}{2}\right]\Gamma^2\left[-1-\frac{1}{\beta}-\frac{\gamma}{\beta}\right]} \left(\frac{R}{R_0}\right)^{1-2\beta}, \qquad \beta < 0, \tag{38}$$

$$T(R) = \frac{2\pi\Sigma_0 v_0^2 R_0^2}{1+\gamma} \frac{\Gamma^2\left[1+\frac{\gamma}{2}\right]}{\Gamma^2\left[\frac{1}{2}+\frac{\gamma}{2}\right]} \left(\frac{R}{R_0}\right), \qquad \beta = 0. \tag{39}$$

This concludes our summary of the equilibrium distribution functions for the power-law disks. In passing, let us emphasise that they are just the simplest choice of distribution functions, not the only ones. To illustrate this, Appendix A gives an example of a very different set of distribution functions. These perhaps fall into the class of remarkable curiosities, since the disks are built from orbits of one shape only.

2.5 The Cut-Out Distribution Functions

So far we have considered only the self-consistent case. We also plan to examine disks where parts of the central density are carved out. This is very much in the spirit of Zang's (1976) pioneering investigations. The cut-out mass is still present, in the sense that it contributes to the forces experienced by the remaining stars, but it is not free to participate in the perturbation. The disk is thus divided into "active" and "inactive" components. Although motivated partly by mathematical convenience, this is also a physically reasonable step to take. Stars in galactic disks are subject not merely to the disk's gravity field, but also to forces from the halo and bulge. A self-consistent distribution function, such as $f_{\rm s}$, is appropriate only when the disk's self-gravity overwhelms the gravitational potential of the other components. The immobile central mass can be interpreted physically as the hot bulge at the centre of disk galaxies. Another possibility – suggested to us by Tremaine (1997, private communication) – is to interpret the rigid density as caused by stars on highly elongated radial orbits. They pass through the centre of the disk, but they spend most of their time sufficiently far away from the disk so that they do not respond to the changing potential. There is one further motivation to consider cut-out disks as well as self-consistent ones. We wish to compare our results with those from N-body studies – for example, those of Sellwood, Earn and collaborators (Sellwood & Athanassoula 1986; Earn 1993; Earn & Sellwood 1995). Obviously, numerical simulations cannot cope with infinite forces so in these studies the singularity at the origin is softened. Although some simulations (e.g., using Bessel function expansions) can track the behaviour of stars to infinite distances, disks with infinite mass are still problematic. For this reason, the disk is truncated at some finite radius. For comparison with these studies, an outer cut-out is needed, as well as an inner one.

To ensure that we do not run afoul of Jeans' (1919) theorem, the carving-out is performed by multiplying our self-consistent distribution function $f_{\rm s}$ (26) by a cut-out function $H(L_z)$:

$$f_{\rm cutout}(E, L_z) = H(L_z) f_{\rm s}(E, L_z). \tag{40}$$

We carry out our analysis for three cut-out functions $H(L_z)$: the self-consistent (scale-free) disk, the inner cut-out disk and the doubly cut-out disk. These are given respectively by

$$H(L_z) = 1, \qquad H(L_z) = \frac{L_z^{N_\beta}}{L_z^{N_\beta} + (v_\beta R_0)^{N_\beta}}, \qquad H(L_z) = \frac{L_z^{N_\beta} L_{\rm c}^{M_\beta}}{\left[L_z^{N_\beta} + (v_\beta R_0)^{N_\beta}\right]\left[L_z^{M_\beta} + L_{\rm c}^{M_\beta}\right]}. \tag{41}$$

In Section 3, we will frequently use an equivalent form of the cut-out function expressed in dimensionless variables defined by $\tilde{H}(\tilde{L}_z) \equiv H(L)$. In all these formulae,

$$N_\beta = \frac{2+\beta}{2-\beta} N, \qquad M_\beta = \frac{2+\beta}{2-\beta} M, \tag{42}$$

where N and M are the inner and outer cut-out indices, respectively and must be positive integers. The choice of the inner cut-out reduces to Zang's (1976, eq. Z2.57) when $\beta \to 0$. Our generalisation seems to come "out of thin

air", but we shall see in Section 3.5 and Appendix C that our choice enables the analytic, rather than numerical, evaluation of a contour integral. Earn (1993) uses a doubly cut-out function of the same form as (41) to carry out his numerical simulations (although, not having to perform any contour integrals, Earn is free to choose non-integral N and M).

What effect does this modification of the distribution function have on the surface density? When the disk is cold, the cut-out function depends only on radius and the active surface density may be calculated exactly. For a doubly cut-out disk, it is

$$\frac{\Sigma^{\rm cold}_{\rm active}}{\Sigma_{\rm eq}} = \frac{R^{\frac{2+\beta}{2}N}}{\left[R^{\frac{2+\beta}{2}N} + R_0^{\frac{2+\beta}{2}N}\right]} \frac{(R_0\tilde{R}_{\rm c})^{\frac{2+\beta}{2}M}}{\left[R^{\frac{2+\beta}{2}M} + (R_0\tilde{R}_{\rm c})^{\frac{2+\beta}{2}M}\right]}, \tag{43}$$

where the truncation radius $\tilde{R}_{\rm c}$ is given by $\tilde{R}_{\rm c} = \tilde{L}_{\rm c}^{2/(2-\beta)}$. The proportion of the equilibrium disk which remains active rises from zero at the centre of the disk to unity at larger radii. At $R = R_0$, the inner cut-out removes exactly half the equilbrium density. The value of N controls the steepness of the rise: the cut-out is gentler for smaller values of N. Conversely, the outer cut-out, parametrised by M, removes matter from the outer regions of the disk. At $R = \tilde{R}_c R_0$, it removes half the equilibrium density, with M controlling the sharpness of the cut-out.

The active surface density of a hot disk can be calculated by numerical integration. In fact, heating the disk makes little difference to the active density. Figs. 2 and 3 show the active surface density of inner and doubly cut-out hot disks. In each case, the active surface density is expressed as a fraction of the equilibrium surface density. The form of these curves is close to that of $\tilde{H}(\tilde{L}_z)$. Thus the value of $\tilde{H}(\tilde{L}_z)$ is a good approximation to the proportion of density which is active at $R = R_0\tilde{L}_z$. Our motivation for introducing the outer cut-off is to enable our results to be directly compared against N-body work. In practice, the outer cut-out does not usually have a significant effect on the stability properties of the disk (unless it is so sharp as to provoke edge modes).

3 THE FREDHOLM INTEGRAL EQUATION

This section derives the Fredholm integral equation for the linear normal modes of the power-law disks. The first step is to decompose the imposed density into logarithmic spirals, as in Section 3.1. Linearising the collisionless Boltzmann equation enables us to calculate the density response. The condition for a self-consistent normal mode is that the imposed density equals the response density. This yields the Fredholm integral equation written down in Section 3.2. The kernel of the integral equation is the transfer function, describing how an excitation at any wavenumber feeds into response at all other wavenumbers. The general formulae for the transfer function is derived in Section 3.3. It depends on the properties of the equilibrium disk through the angular momentum function, as discussed in Section 3.4.

3.1 The Logarithmic Spirals

The logarithmic spirals were made famous by Snow (1952) and Kalnajs (1965; 1971). They have surface density

$$\Sigma^{\alpha m}_{\rm imp} = \Sigma_{\rm p} e^{st} e^{im(\theta - \Omega_{\rm p} t)} \left(\frac{R_0}{R}\right)^{3/2 - i\alpha} = \Sigma_{\rm p} e^{i(m\theta - \omega t)} \left(\frac{R_0}{R}\right)^{3/2 - i\alpha}, \tag{44}$$

where $\Sigma_{\rm p}$ is a constant amplitude. This m-lobed pattern rotates with a constant pattern speed $\Omega_{\rm p}$ and grows or decays with a growth rate s. The logarithmic wavenumber (hereafter abbreviated to just wavenumber) α controls how tightly the spiral is wrapped. The pattern is more tightly wound for larger values of α. It is often convenient to collect the growth rate and pattern speed into the complex frequency $\omega = m\Omega_{\rm p} + is$. By adding logarithmic spirals with different α, we can build up general patterns with azimuthal wavenumber m:

$$\Sigma_{\rm imp}(R, \theta) = \int_{-\infty}^{+\infty} d\alpha A_{\rm imp}(\alpha) \Sigma^{\alpha m}_{\rm imp}. \tag{45}$$

Any imposed density perturbation $\Sigma_{\rm imp}$ is expanded in a Fourier series of azimuthal harmonics characterised by m. In the linear régime, the response of the disk to the change in potential has the same order m of rotational symmetry as the imposed density perturbation. This means that our investigations can be confined to a single value of m at a time. The expansion in logarithmic spirals is equivalent to taking the Fourier transform in the variable $\tilde{x} = \ln(R/R_0)$. This is evident on defining

$$\Sigma_m = \Sigma_{\rm p} e^{i(m\theta - \omega t)} e^{-3\tilde{x}/2} \tag{46}$$

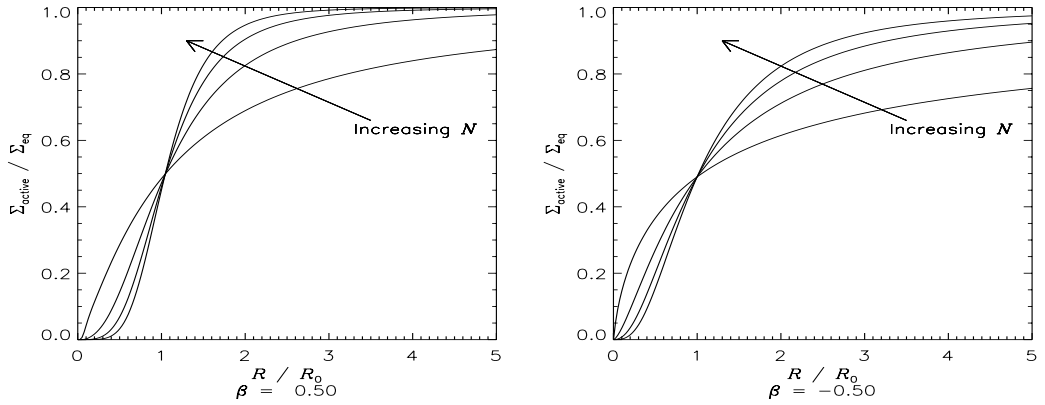

Figure 2. The active surface density of a hot disk with an inner cut-out function, shown as a fraction of the equilibrium density. The cut-out becomes more abrupt with increasing N. [The solid lines are the density for $N = 1$, 2, 3, 4. For $\beta = +0.5$, $\tilde{\sigma}_u = 0.199$; for $\beta = -0.5$, $\tilde{\sigma}_u = 0.740$. These are the temperatures at which the self-consistent disk is locally stable to axisymmetric disturbances.]

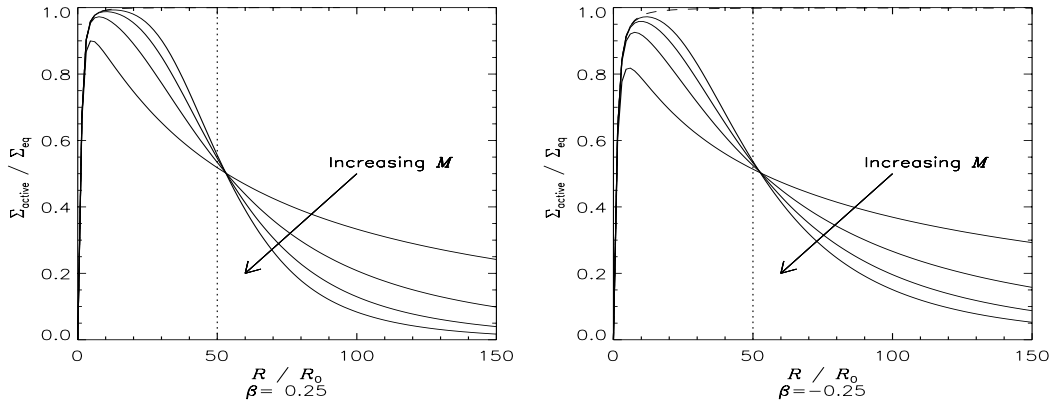

Figure 3. The active surface density of hot disks with a doubly cut-out function, shown as a fraction of the equilibrium density. The arrows indicate the direction of increasing M, or increasing severity of the truncation. The dashed line just visible at the top of the plots is the corresponding inner cut-out disk. [In each case, $N = 2$, $\tilde{R}_c = 50$. The solid lines are the density for $M = 1$, 2, 3, 4. The dotted line marks the position of $\tilde{R}_c$. For $\beta = +0.25$, $\tilde{\sigma}_u = 0.283$; for $\beta = -0.25$,$\tilde{\sigma}_u = 0.509$.]

so that we obtain the conventional Fourier transform pair:

$$\frac{\Sigma_{\rm imp}}{\Sigma_m} = \int_{-\infty}^{+\infty} d\alpha\, A_{\rm imp}\,(\alpha)\, e^{i\alpha\tilde{x}}, \qquad\qquad A_{\rm imp}\,(\alpha) = \frac{1}{2\pi}\int_{-\infty}^{+\infty} d\tilde{x}\, \frac{\Sigma_{\rm imp}}{\Sigma_m} e^{-i\alpha\tilde{x}}. \tag{47}$$

Here, $A_{\rm imp}$ is the Fourier transform of the imposed density perturbation. For the transform to exist, $\Sigma_{\rm imp}\,(R,\theta)\,R^{3/2}$ must tend to zero as $R \to 0$ and $R \to \infty$. This means that $\Sigma_{\rm imp}\,(R,\theta)$ can diverge at the centre no faster than $R^{-3/2}$ and must fall off at large radii more quickly than $R^{-3/2}$. Kalnajs (1965; 1971) derived the potential $\psi^{\alpha m}_{\rm imp}$ corresponding to a single logarithmic spiral component $\Sigma^{\alpha m}_{\rm imp}$ as

$$\psi^{\alpha m}_{\rm imp} = 2\pi G \Sigma_{\rm p} K(\alpha, m) R_0 e^{i(m\theta - \omega t)} \left(\frac{R}{R_0}\right)^{i\alpha - \frac{1}{2}}, \tag{48}$$

where $K(\alpha, m)$ is the Kalnajs gravity function

$$K(\alpha, m) = \frac{1}{2}\frac{\Gamma\left[\frac{1}{2}\left(\frac{1}{2} + m + i\alpha\right)\right]\Gamma\left[\frac{1}{2}\left(\frac{1}{2} + m - i\alpha\right)\right]}{\Gamma\left[\frac{1}{2}\left(\frac{3}{2} + m + i\alpha\right)\right]\Gamma\left[\frac{1}{2}\left(\frac{3}{2} + m - i\alpha\right)\right]}. \tag{49}$$

This function is real and positive for real α. It has the symmetry $K(\alpha, m) = K(-\alpha, m)$.

From the imposed potential $\psi^{\alpha m}_{\rm imp}$, we obtain the change in the distribution function $f^{\alpha m}_{\rm imp}$. The linearised collisionless Boltzmann equation (Binney & Tremaine 1987, chap. 5) relates the change in the distribution function to the changes in energy and angular momentum experienced by individual stars as a result of the density perturbation:

$$\frac{df_{\rm imp}}{dt} = -\left(u\frac{\partial\psi_{\rm imp}}{\partial R} + \frac{v}{R}\frac{\partial\psi_{\rm imp}}{\partial\theta}\right)\frac{\partial f}{\partial E} - \frac{\partial\psi_{\rm imp}}{\partial\theta}\frac{\partial f}{\partial L_z} = -\frac{\partial f}{\partial E}\frac{dE}{dt} - \frac{\partial f}{\partial L_z}\frac{dL_z}{dt}. \tag{50}$$

In physical terms, eq. (50) simply states that the rate at which stars move to perturbed orbits is equal to the rate at which stars leave equilibrium orbits. Integrating (50) over the entire time of the perturbation, we obtain

$$f^{\alpha m}_{\rm imp}(t) = -\frac{\partial f}{\partial E}\Delta E - \frac{\partial f}{\partial L_z}\Delta L_z, \tag{51}$$

where ΔE and ΔL_z are the changes in the star's energy and angular momentum due to the perturbation. For a single logarithmic spiral component, these simplify to

$$\Delta E = \int_{-\infty}^{t}\left(u'\frac{\partial \psi^{\alpha m}_{\rm imp}}{\partial R'} + \frac{v'}{R'}\frac{\partial \psi^{\alpha m}_{\rm imp}}{\partial \theta'}\right)dt' = \psi^{\alpha m}_{\rm imp}(t) - \int_{-\infty}^{t}\frac{\partial \psi^{\alpha m}_{\rm imp}}{\partial t'}dt'. \qquad \Delta L_z = \int_{-\infty}^{t}\frac{\partial \psi^{\alpha m}_{\rm imp}}{\partial \theta'}dt'. \tag{52}$$

Physically, ΔE is the difference between the potential here and now, and an averaged potential sampled by the orbit over its history. Note that this derivation assumes that the perturbation vanished in the distant past.

3.2 The Integral Equation

To find the change in surface density $\Sigma^{\alpha m}_{\rm res}$ caused by a single logarithmic spiral component $\Sigma^{\alpha m}_{\rm imp}$, an integration of $f^{\alpha m}_{\rm imp}$ must be performed over all velocities u and v

$$\Sigma^{\alpha m}_{\rm res} = \iint f^{\alpha m}_{\rm imp}\, du\, dv. \tag{53}$$

To find the total change in density caused by the whole disturbance $\Sigma_{\rm imp} = \int d\alpha\, A_{\rm imp}(\alpha)\, \Sigma^{\alpha m}_{\rm imp}$, we integrate over all the logarithmic spiral components

$$\Sigma_{\rm res} = \int_{-\infty}^{+\infty} d\alpha\, A_{\rm imp}(\alpha)\, \Sigma^{\alpha m}_{\rm res}. \tag{54}$$

It is possible to equate $\Sigma_{\rm res}$ and $\Sigma_{\rm imp}$ and seek to solve the resulting equation for the self-consistent solutions. A more profitable approach is to equate the density transforms. We define the response density transform $A_{\rm res}(\alpha)$ analogously to (47) so that

$$\frac{\Sigma_{\rm res}}{\Sigma_m} = \int_{-\infty}^{+\infty} d\alpha\, A_{\rm res}(\alpha)\, e^{i\alpha\tilde{x}}, \qquad A_{\rm res}(\alpha) = \frac{1}{2\pi}\int_{-\infty}^{+\infty} d\tilde{x}\, \frac{\Sigma_{\rm res}}{\Sigma_m} e^{-i\alpha\tilde{x}}. \tag{55}$$

Substituting for $\Sigma_{\rm res}$ from (54), the response density transform becomes

$$A_{\rm res}(\alpha) = \frac{1}{2\pi}\int_{-\infty}^{+\infty} d\tilde{x}\, \frac{e^{-i\alpha\tilde{x}}}{\Sigma_m}\int_{-\infty}^{+\infty} d\alpha' A_{\rm imp}(\alpha')\, \Sigma^{\alpha' m}_{\rm res}. \tag{56}$$

Exchanging the order of integration, we obtain (cf. Z3.42):

$$A_{\rm res}(\alpha) = \int_{-\infty}^{+\infty} d\alpha' A_{\rm imp}(\alpha')\, \mathcal{S}_m(\alpha,\alpha'), \qquad \text{where} \qquad \mathcal{S}_m(\alpha,\alpha') = \frac{1}{2\pi}\int_{-\infty}^{+\infty} d\tilde{x}\, \frac{\Sigma^{\alpha' m}_{\rm res}}{\Sigma_m} e^{-i\alpha\tilde{x}}. \tag{57}$$

Self-consistency requires the response density to equal the imposed density, or equivalently $A_{\rm imp}(\alpha) = A_{\rm res}(\alpha)$. Equation (57) therefore becomes an integral equation for the density transform of the normal modes of oscillation. Of course, similar integral equations have been derived by others before. For example, Kalnajs (1971) derived a completely general integral equation in action-angle coordinates, whereas Palmer & Papaloizou (1990) restricted their attention to disks built from epicyclic orbits. This form of the integral equation was first derived by Zang (1976). The kernel of the integral equation $\mathcal{S}_m(\alpha,\alpha')$ is called the *transfer function* and describes how much of the disks response to the disturbance with wavenumber α' occurs at the wavenumber α. It is to the transfer function that our attention now turns.

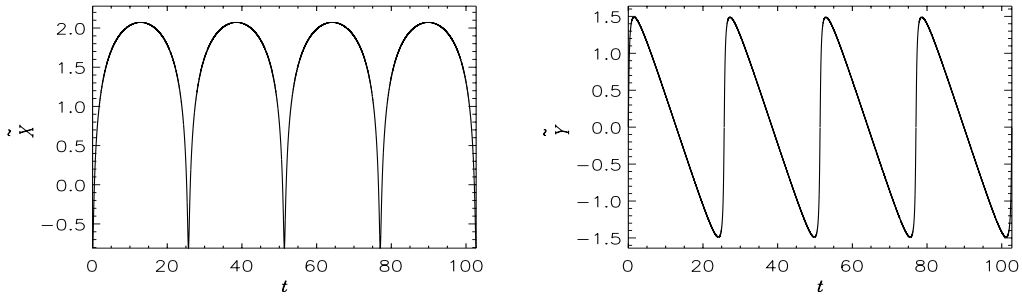

Figure 4. Excursions of a stellar orbit as viewed in the $\tilde{X}$ and $\tilde{Y}$ coordinates. The left panel shows the scaled logarithmic radius $\tilde{X}$ and the right panel the deviation from mean angular motion $\tilde{Y}$ plotted against time. [Numerical details: $U = 1.5$, $R_H = 1$, $\beta = 0.25$, $R_0 = v_\beta = 1$.]

3.3 The Transfer Function

This section contains an elaborate calculation of the transfer function of the power-law disks. To aid the reader, a reference table of some of the quantities are collected in Appendix B. The first step is to evaluate the change in distribution function $f^{\alpha m}_{\rm imp}$ given in eq. (51). From eqs. (48) and (52), the changes in energy and angular momentum caused by a single logarithmic spiral component are

$$\Delta E = \psi^{\alpha m}_{\rm imp}(t) + i\omega \int_{-\infty}^{t} \psi^{\alpha m}_{\rm imp}\,(t')\,dt', \qquad\qquad \Delta L_z = im \int_{-\infty}^{t} \psi^{\alpha m}_{\rm imp}\,(t')\,dt'. \tag{58}$$

The integration is simplified by shifting to the frame which rotates at the star's average velocity Ω. In this frame, the star's orbit closes and the integrands in eq. (58) become periodic with the radial period T. Following Zang (1976), let us define two dimensionless coordinates describing the periodic excursions of the stellar orbits as:

$$\tilde{X} = \ln \frac{R}{R_H} = \ln \tilde{R}, \qquad\qquad \tilde{Y} = \theta - \Omega t = \theta - \tilde{\Omega}\tilde{t}. \tag{59}$$

Fig. 4 shows how $\tilde{X}$ and $\tilde{Y}$ vary over four radial periods for a somewhat eccentric orbit. The potential $\psi_{\rm imp}$ (48) experienced by the star at time t' when its position is (R', θ'), or equivalently $\tilde{X}' = \ln \tilde{R}'$, $\tilde{Y}' = \theta' - \Omega t'$, is:

$$\psi^{\alpha m}_{\rm imp}(t') = 2\pi G \Sigma_{\rm p} K(\alpha, m) R_0 \tilde{R}_H^{i\alpha - \frac{1}{2}} \exp\left\{ i(m\Omega - \omega)t' + im\tilde{Y}' + (i\alpha - \tfrac{1}{2})\tilde{X}' \right\}. \tag{60}$$

Now $\tilde{X}$ and $\tilde{Y}$ both have period T, so the term $\exp\left\{ im\tilde{Y}' + (i\alpha - \frac{1}{2})\tilde{X}' \right\}$ is similarly periodic as t' varies. It can therefore be expanded in a Fourier series (a method previously used by Kalnajs (1972) and Zang (1976)):

$$\exp\left\{ im\tilde{Y}' + (i\alpha - \tfrac{1}{2})\tilde{X}' \right\} = \sum_{l=-\infty}^{+\infty} Q_{lm}(\alpha) \exp\left\{ \frac{2i\pi l}{T} t' \right\}, \tag{61}$$

where the Fourier coefficient $Q_{lm}(\alpha)$ is given by

$$Q_{lm}(\alpha) = \frac{1}{T} \int_0^T \exp\left\{ im\tilde{Y}' + (i\alpha - \tfrac{1}{2})\tilde{X}' - \frac{2i\pi l}{T} t' \right\} dt'. \tag{62}$$

Changing variables to the orbital phase $\chi = \kappa t$, the Fourier coefficient becomes (Z3.27)

$$Q_{lm}(\alpha) = \frac{1}{2\pi} \int_0^{2\pi} \exp\left\{ im\tilde{Y}' + (i\alpha - \tfrac{1}{2})\tilde{X}' - il\chi' \right\} d\chi'. \tag{63}$$

Substituting this into our expression (60), we obtain for the perturbation potential sampled by the star

$$\psi^{\alpha m}_{\rm imp}(t') = 2\pi G \Sigma_{\rm p} K(\alpha, m) R_0 \tilde{R}_H^{i\alpha - \frac{1}{2}} e^{i(m\Omega - \omega)t'} \sum_{l=-\infty}^{+\infty} Q_{lm}(\alpha) e^{il\kappa t'}. \tag{64}$$

Using (58), the changes in the energy and the angular momentum of the star caused by a single logarithmic spiral is

$$\Delta E = 2\pi G\Sigma_{\rm p} K(\alpha,m) R_0 \tilde{R}_H^{i\alpha-\frac{1}{2}} e^{i(m\Omega-\omega)t} \sum_{l=-\infty}^{+\infty} Q_{lm}(\alpha) e^{il\chi} \frac{l\kappa+m\Omega}{l\kappa+m\Omega-\omega}, \tag{65}$$

$$\Delta L_z = 2\pi m G\Sigma_{\rm p} K(\alpha,m) R_0 \tilde{R}_H^{i\alpha-\frac{1}{2}} e^{i(m\Omega-\omega)t} \sum_{l=-\infty}^{+\infty} \frac{Q_{lm}(\alpha) e^{il\chi}}{l\kappa+m\Omega-\omega}. \tag{66}$$

These correspond to (Z3.29) and (Z3.30), although Zang uses a slightly different form of the Fourier coefficient. Substituting these expressions into (51) gives the final expression for the change in the distribution function:

$$f_{\rm imp}^{\alpha m}(t) = -2\pi G\Sigma_{\rm p} K(\alpha,m) R_0 \tilde{R}_H^{i\alpha-\frac{1}{2}} e^{i(m\Omega-\omega)t} \sum_{l=-\infty}^{+\infty} \frac{Q_{lm}(\alpha) e^{il\chi}}{l\kappa+m\Omega-\omega} \left\{ (l\kappa+m\Omega)\frac{\partial f}{\partial E} + m\frac{\partial f}{\partial L_z} \right\}. \tag{67}$$

Thus far, our results are independent of the form of the equilibrium disk. Let us now specialise to the power-law disks by substituting for the derivatives of the distribution function (40). Bearing in mind that the energy E has the opposite sign to β, we can combine the derivatives obtained for positive and negative β.

$$\frac{\partial f}{\partial E} = -\tilde{C}\left|\frac{1}{\beta}+\frac{\gamma}{\beta}-\frac{\gamma}{2}\right| H(L_z) L_z^{\gamma} |E|^{1/\beta+\gamma/\beta-\gamma/2-1}, \qquad \frac{\partial f}{\partial L_z} = \tilde{C} L_z^{\gamma} |E|^{1/\beta+\gamma/\beta-\gamma/2} \left(\gamma\frac{H(L_z)}{L_z} + \frac{dH}{dL_z}\right). \tag{68}$$

We also replace the dimensional quantities with their dimensionless analogues (eqs. (12), (22), (24))

$$L_z = v_\beta R_0 \tilde{L}_z, \qquad \frac{dH}{dL_z} = \frac{1}{v_\beta R_0}\frac{d\tilde{H}}{d\tilde{L}_z}, \qquad E = \tilde{E} v_\beta^2 \tilde{L}_z^{\frac{2\beta}{\beta-2}}, \tag{69}$$

$$\kappa = \tilde{\kappa}\frac{v_\beta}{R_0}\tilde{L}_z^{\frac{2+\beta}{\beta-2}}, \qquad \Omega = \tilde{\Omega}\frac{v_\beta}{R_0}\tilde{L}_z^{\frac{2+\beta}{\beta-2}}, \qquad \omega = \tilde{\omega}\frac{v_\beta}{R_0}, \tag{70}$$

Note that $\tilde{\omega}$ is defined slightly differently from $\tilde{\kappa}$ and $\tilde{\Omega}$. With the present definitions, all three dimensionless frequencies are independent of $\tilde{L}_z$ (it is clear from eqs. (22), (24) and (18) that $\tilde{\kappa}$ and $\tilde{\Omega}$ depend only on $\tilde{U}$). With these substitutions, the change in the distribution function now becomes

$$\begin{aligned} f_{\rm imp}^{\alpha m}(t) = {} & 2\pi G\Sigma_{\rm p} K(\alpha,m)\tilde{C} R_0^{\gamma+1} v_\beta^{\frac{2}{\beta}(1+\gamma)-2} e^{i(m\Omega-\omega)t} e^{i\alpha\frac{2}{2-\beta}\ln\tilde{L}_z} \tilde{L}_z^{\frac{2\beta-3}{2-\beta}} |\tilde{E}|^{1/\beta+\gamma/\beta-\gamma/2} \\ & \times \sum_{l=-\infty}^{\infty} \frac{Q_{lm}(\alpha) e^{il\chi}}{l\tilde{\kappa}+m\tilde{\Omega}-\tilde{\omega}\tilde{L}_z^{\frac{2+\beta}{2-\beta}}} \left[\left\{ (l\tilde{\kappa}+m\tilde{\Omega}) \left|\frac{1}{\beta}+\frac{\gamma}{\beta}-\frac{\gamma}{2}\right| \frac{1}{|\tilde{E}|} - \gamma m \right\} \tilde{H}(\tilde{L}_z) - m\tilde{L}_z\frac{d\tilde{H}}{d\tilde{L}_z} \right]. \end{aligned} \tag{71}$$

This is the change in the distribution function brought about by a single logarithmic spiral component.

Let us now proceed to find the transfer function $\mathcal{S}_m$ from (57). Substituting for the response surface density in terms of the response distribution function, we have:

$$\mathcal{S}_m(\alpha,\alpha') = \frac{1}{2\pi}\int_{-\infty}^{+\infty} d\tilde{x}\, \frac{e^{-i\alpha\tilde{x}}}{\Sigma_m} \iint f_{\rm imp}^{\alpha' m}\, du\, dv. \tag{72}$$

This triple integral is transformed to one over the eccentric velocity $\tilde{U}$, the orbital phase χ and the dimensionless angular momentum $\tilde{L}_z$. A careful calculation of the Jacobian (Read 1997) reveals:

$$\frac{\partial(\tilde{x},u,v)}{\partial(\chi,\tilde{U},\tilde{L}_z)} = \frac{v_\beta^2}{2\pi}\frac{\mathcal{J}_0(\tilde{U})\tilde{U}}{\tilde{R}} e^{-\tilde{x}} \tilde{L}_z^{\frac{\beta}{\beta-2}}. \tag{73}$$

The transfer function then becomes

$$\mathcal{S}_m(\alpha,\alpha') = \frac{v_\beta^2}{2\pi}\iiint d\tilde{U}\, d\chi\, d\tilde{L}_z \frac{e^{-(i\alpha+1)\bar{x}}}{\Sigma_m}\frac{\mathcal{J}_0(\tilde{U})}{2\pi}\frac{\tilde{U}}{\tilde{R}}\tilde{L}_z^{\frac{\beta}{\beta-2}} f_{\rm imp}^{\alpha' m}(\tilde{L}_z,\tilde{U},\chi). \tag{74}$$

The angular momentum is integrated from zero to infinity, and the orbital phase from 0 to 2π. The eccentric velocity

is integrated from zero to infinity for negative β; for positive β the upper limit is $(2/\beta-1)^{1/2}$. For brevity, these limits of the integration are not shown explicitly.

We shall work in terms of $\tilde{X}=\ln\tilde{R}=\ln(R/R_H)=\tilde{x}-\frac{2}{2-\beta}\ln\tilde{L}_z$. Then $\tilde{R}=e^{\tilde{X}}$, and on substituting for Σ_m from (46) we obtain

$$\mathcal{S}_m(\alpha,\alpha')=\frac{v_\beta^2}{2\pi\Sigma_{\rm p}}\frac{1}{2\pi}\iiint d\tilde{U}\,d\chi\,d\tilde{L}_z e^{-i(m\theta-\omega t)}e^{-(i\alpha+\frac{1}{2})\tilde{X}}e^{\frac{1-\beta-2i\alpha}{2-\beta}\ln\tilde{L}_z}\mathcal{J}_0(\tilde{U})\tilde{U}f_{\rm imp}^{\alpha' m}(\tilde{L}_z,\tilde{U},\chi). \tag{75}$$

Note that t, $\tilde{X}$ and θ describe where the star is in its orbit. They therefore depend on the orbital phase χ, as well as on $\tilde{U}$ which describes the shape of the orbit. Substituting for $f_{\rm imp}^{\alpha' m}$ from (71):

$$\begin{aligned}\mathcal{S}_m(\alpha,\alpha')=R_0^{\gamma+1}v_\beta^{\frac{2}{\beta}(1+\gamma)}\frac{GK(\alpha',m)\tilde{C}}{2\pi}\iiint d\tilde{U}\,d\chi\,\frac{d\tilde{L}_z}{\tilde{L}_z}e^{-im(\theta-\Omega t)}e^{-(i\alpha+\frac{1}{2})\tilde{X}}e^{\frac{-2i}{2-\beta}(\alpha-\alpha')\ln\tilde{L}_z}\tilde{U}\mathcal{J}_0(\tilde{U})|\tilde{E}|^{\frac{1}{\beta}+\frac{\gamma}{\beta}-\frac{\gamma}{2}}\\ \times\sum_{l=-\infty}^{+\infty}\frac{Q_{lm}(\alpha')e^{il\chi}}{l\tilde{\kappa}+m\tilde{\Omega}-\tilde{\omega}\tilde{L}_z^{\frac{2+\beta}{2-\beta}}}\left[\left\{(l\tilde{\kappa}+m\tilde{\Omega})\left|\frac{1}{\beta}+\frac{\gamma}{\beta}-\frac{\gamma}{2}\right|\frac{1}{|\tilde{E}|}-\gamma m\right\}\tilde{H}(\tilde{L}_z)-m\tilde{L}_z\frac{d\tilde{H}}{d\tilde{L}_z}\right].\end{aligned} \tag{76}$$

Substituting $\tilde{E}=(\beta\tilde{U}^2+\beta-2)/(2\beta)$ and $\theta-\Omega t=\tilde{Y}(\chi)$,

$$\begin{aligned}\mathcal{S}_m(\alpha,\alpha')=R_0^{\gamma+1}v_\beta^{\frac{2}{\beta}(1+\gamma)}2\pi GK(\alpha',m)\tilde{C}\int d\tilde{U}\mathcal{J}_0(\tilde{U})\tilde{U}\left|\frac{\beta\tilde{U}^2+\beta-2}{2\beta}\right|^{\frac{1}{\beta}+\frac{\gamma}{\beta}-\frac{\gamma}{2}}\\ \times\sum_{l=-\infty}^{+\infty}Q_{lm}(\alpha')\frac{1}{2\pi}\int d\chi e^{il\chi-im\tilde{Y}-(i\alpha+\frac{1}{2})\tilde{X}}\\ \times\frac{1}{2\pi}\int\frac{d\tilde{L}_z}{\tilde{L}_z}\frac{e^{\frac{-2i}{2-\beta}(\alpha-\alpha')\ln\tilde{L}_z}}{l\tilde{\kappa}+m\tilde{\Omega}-\tilde{\omega}\tilde{L}_z^{\frac{2+\beta}{2-\beta}}}\left[\left\{(l\tilde{\kappa}+m\tilde{\Omega})\left|\frac{2+2\gamma-\beta\gamma}{\beta\tilde{U}^2+\beta-2}\right|-\gamma m\right\}\tilde{H}(\tilde{L}_z)-m\tilde{L}_z\frac{d\tilde{H}}{d\tilde{L}_z}\right].\end{aligned} \tag{77}$$

From the definition of the Fourier coefficient (63), the integral over orbital phase χ is just the complex conjugate of $Q_{lm}(\alpha)$. Then, the transfer function becomes:

$$\mathcal{S}_m(\alpha,\alpha')=R_0^{\gamma+1}v_\beta^{\frac{2}{\beta}(1+\gamma)}2\pi GK(\alpha',m)\tilde{C}\int d\tilde{U}\mathcal{J}_0(\tilde{U})\tilde{U}\left|\frac{\beta\tilde{U}^2+\beta-2}{2\beta}\right|^{\frac{1}{\beta}+\frac{\gamma}{\beta}-\frac{\gamma}{2}}\sum_{l=-\infty}^{+\infty}Q_{lm}(\alpha')Q_{lm}^*(\alpha)F_{lm}(\alpha-\alpha'). \tag{78}$$

Here, to make this expression a little more manageable, we have defined the integral over angular momentum to be the *angular momentum function* $F_{lm}(\eta)$, where $\eta=\alpha-\alpha'$:

$$F_{lm}(\eta)=\frac{1}{2\pi}\int_0^\infty\frac{e^{-i\eta\frac{2}{2-\beta}\ln\tilde{L}_z}}{l\tilde{\kappa}+m\tilde{\Omega}-\tilde{\omega}\tilde{L}_z^{\frac{2+\beta}{2-\beta}}}\left[\left\{(l\tilde{\kappa}+m\tilde{\Omega})\left|\frac{2+2\gamma-\beta\gamma}{\beta\tilde{U}^2+\beta-2}\right|-\gamma m\right\}\tilde{H}(\tilde{L}_z)-m\tilde{L}_z\frac{d\tilde{H}}{d\tilde{L}_z}\right]\frac{d\tilde{L}_z}{\tilde{L}_z}. \tag{79}$$

For convenience, the Fourier coefficients Q_{lm} and the angular momentum function F_{lm} are shown as depending only upon the wavenumber α in (78), although they also depend upon the eccentric velocity $\tilde{U}$ as well as on the disk parameters. The corresponding results for the transfer function and the angular momentum function for the Toomre-Zang disk are (Z3.40):

$$\mathcal{S}_m(\alpha,\alpha')=\frac{(\gamma+1)^{1+\gamma/2}K(\alpha',m)}{2^{\gamma/2}e^{(\gamma+1)/2}\sqrt{\pi}\Gamma\left[\frac{\gamma+1}{2}\right]}\left(\frac{2}{\gamma+1}\right)^{\gamma/2}\int d\tilde{U}\,\mathcal{J}_0(\tilde{U})\tilde{U}e^{-\frac{(\gamma+1)\tilde{U}^2}{2}}\sum_{l=-\infty}^{+\infty}Q_{lm}(\alpha')Q_{lm}^*(\alpha)F_{lm}(\alpha-\alpha'). \tag{80}$$

$$F_{lm}=\frac{1}{2\pi}\int_0^\infty\frac{e^{-i\eta\ln\tilde{L}_z}}{l\tilde{\kappa}+m\tilde{\Omega}-\tilde{\omega}\tilde{L}_z}\left[\left\{(l\tilde{\kappa}+m\tilde{\Omega})(1+\gamma)-\gamma m\right\}\tilde{H}(\tilde{L}_z)-m\tilde{L}_z\frac{d\tilde{H}}{d\tilde{L}_z}\right]\frac{d\tilde{L}_z}{\tilde{L}_z}. \tag{81}$$

Can we gain some rather more intuitive understanding of this complicated expression for $\mathcal{S}_m$? The transfer function $\mathcal{S}_m(\alpha,\alpha')$ describes the contribution of the imposed logarithmic spiral component with wavenumber α' to the response component with wavenumber α. To see how this is calculated, we consider a star orbiting in the disk. The shape

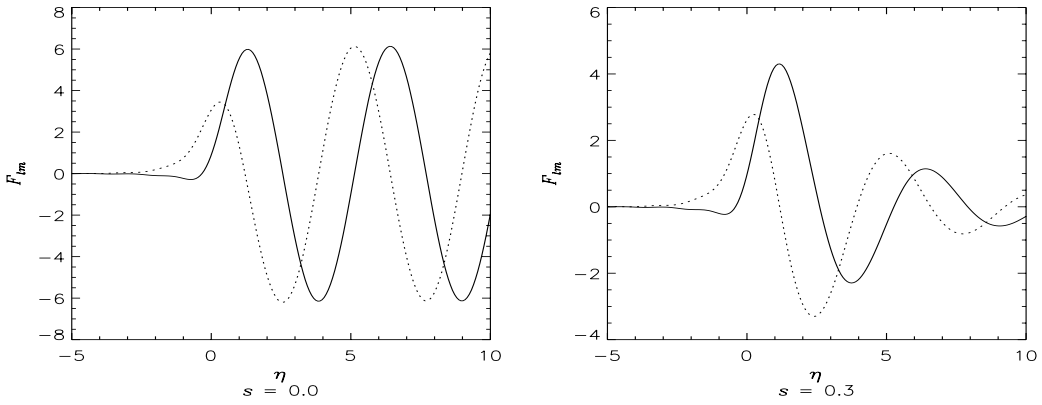

Figure 5. Graph of the angular momentum function F_{22} plotted against η for two different growth rates in a $\beta = 0.25$ disk. In the left panel, $s = 10^{-7}$; on the right, $s = 0.3$. In each case, the solid line is the real part, and the dotted line the imaginary. [Numerical details: $\beta = 0.25$, $N = 2$, $M = 6$, $\tilde{L}_{\rm c} = 31.6$; $\gamma = 13.7$, $\Omega_{\rm p} = 0.5$, $m = 2$; $l = 2$, $\tilde{U} = 0.5$.]

of its orbit is characterised by its eccentric velocity $\tilde{U}$. The Fourier coefficient Q_{lm} describes the "match" between a particular logarithmic spiral component and this orbit. Specifically, the changes in the star's energy and angular momentum caused by the logarithmic spiral perturbation are expanded in harmonics of the orbit's radial period. The Fourier coefficient Q_{lm} gives the contribution to the lth component of the perturbation experienced by the star. Thus, in the expression for the transfer function (78), the first Fourier coefficient $Q_{lm}(\alpha')$ describes how far the star is forced out of its unperturbed orbit by the imposed perturbation, and hence the star's tendency to stop contributing to the imposed logarithmic spiral. The second Fourier coefficient $Q^*_{lm}(\alpha)$ describes how well matched the perturbed star is to the response logarithmic spiral component with wavenumber α. Both these depend only on the shape of the star's orbit, not on its size; nor has any consideration yet been made of the "interaction" between the logarithmic spirals. This is accounted for by the angular momentum function F_{lm}. How easy it is for a star to move from the imposed to the response logarithmic spiral depends on the difference between the response and imposed wavenumbers, $\eta = \alpha - \alpha'$, as well as the charactistics of the perturbation (its azimuthal symmetry, growth rate and pattern speed, given by m and $\tilde{\omega}$), and also on the size of the orbit, $\tilde{L}_z$. The integral in the angular momentum adds up similar-shaped orbits of all different sizes. F_{lm} then describes how feasible it is for density to move from wavenumber α' to α in a perturbation with this m and $\tilde{\omega}$. Owing to the scale-free nature of the disk, we have been able to deal simultaneously with all orbits of a given shape, irrespective of their size. The $\tilde{U}$-dependent parts of the integrand in $\mathcal{S}_m$ measure how many stars there are for each shape of orbit. These are then added up to determine how much density ultimately moves from the logarithmic spiral component with wavenumber α' to that with wavenumber α.

3.4 The Angular Momentum Function

Our job is not quite yet complete! The angular momentum function eq. (79) can be worked out analytically for the cut-out functions $\tilde{H}(\tilde{L}_z)$ given in section 2.5. This contour integration is by no means trivial and it seems wise to relegate the details of the calculation to Appendix C. In this section, we aim to understand the behaviour of the analytic expression for the angular momentum function in physical terms. Fig. 5 compares the angular momentum function for two different growth rates s. The left-hand plot shows $F_{lm}(\eta)$ for vanishing growth rate, while the right-hand one has $s = 0.3$. This figure exemplifies the trailing bias of these disks. Where $l\tilde{\kappa} + m\tilde{\Omega}$ is positive and the eccentric velocity is low, the angular momentum function is highly asymmetric about $\eta = 0$: the decay for $\eta > 0$ is greatly attenuated. For negative values of $l\tilde{\kappa} + m\tilde{\Omega}$ or for high eccentric velocities, F_{lm} decays rapidly as $|\eta|$ moves away from zero in either direction. The mathematical origin of this asymmetry is seen most simply in the expression for F_{lm} in the case of a scale-free disk (C9). This depends on η as

$$F_{lm}(\eta) \propto \frac{e^{-i\hat{\eta}\ln\frac{l\tilde{\kappa}+m\tilde{\Omega}}{\tilde{\omega}}}}{1 - e^{2\pi\hat{\eta}}}, \tag{82}$$

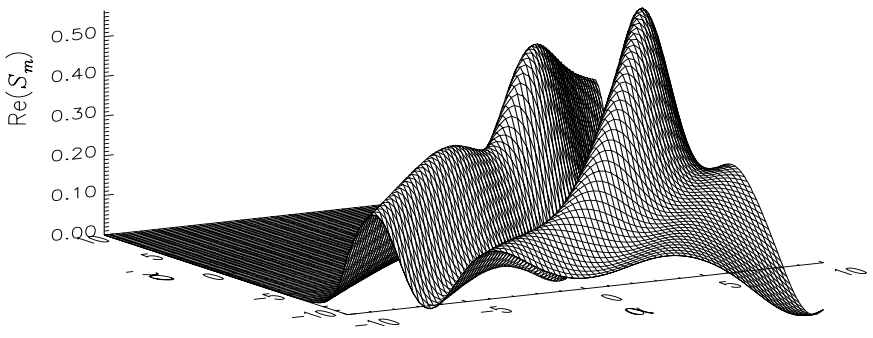

Figure 6. Plot of the real part of the transfer function against α and α'. Notice the abrupt change on crossing the line $\alpha = \alpha'$ – this is the trailing bias. [Numerical details: $\beta = 0.25$, $N = 2$, $M = 6$, $\tilde{L}_c = 31.6$; $\gamma = 13.7$, $\Omega_p = 0.5$, $s = 10^{-7}$, $m = 2$.]

where $\hat{\eta}$ is defined as $2\eta/(2+\beta)$ (see Appendix C, (C4)). If the growth rate is zero, then on taking the principal value of the logarithm, we obtain

$$F_{lm}(\eta) \propto e^{-i\hat{\eta}\ln\left|\frac{l\tilde{\kappa}+m\tilde{\Omega}}{m\Omega_p}\right|}\frac{e^{2\pi\hat{\eta}}}{1-e^{2\pi\hat{\eta}}}, \qquad l\tilde{\kappa}+m\tilde{\Omega}>0; \tag{83}$$

$$F_{lm}(\eta) \propto e^{-i\hat{\eta}\ln\left|\frac{l\tilde{\kappa}+m\tilde{\Omega}}{m\Omega_p}\right|}\frac{e^{\pi\hat{\eta}}}{1-e^{2\pi\hat{\eta}}}, \qquad l\tilde{\kappa}+m\tilde{\Omega}<0. \tag{84}$$

Considering extreme values of η on either side of zero, it is apparent that for $l\tilde{\kappa}+m\tilde{\Omega}>0$ the angular momentum function is be asymmetric about $\eta = 0$. The magnitude of F_{lm} tends to a constant value for large positive η, whereas it decays rapidly as $\exp(-2\pi|\hat{\eta}|)$ for negative η. Conversely, for $l\tilde{\kappa}+m\tilde{\Omega}<0$ no such asymmetry is apparent; F_{lm} decays as $\exp(-\pi|\hat{\eta}|)$ in either direction. After the summation over radial harmonics and integration over eccentric velocity, the magnitude of F_{lm} is likely, on average, to be greater for positive η ($\alpha > \alpha'$) than for negative. This in turn means that, typically, the magnitude of the transfer function $\mathcal{S}_m(\alpha,\alpha')$ is greater for $\alpha > \alpha'$, as demonstrated in fig. 6. Most of the response at α is due to imposed components with wavenumber *less* than α. An alternative way of viewing the situation is that imposed components mostly go to make up response components with *larger* wavenumber than their own. Thus the asymmetry in the transfer function means that our disk tends to make whatever pattern is imposed on it more trailing.

3.5 The Special Case of Axisymmetry

In the case of an axisymmetric perturbation, the integral equation admits certain symmetries. The first simplification is that the frequency is purely imaginary: $\omega = is$. Secondly, the integral equation is equivalent to one with a Hermitian kernel, and hence must have purely real eigenvalues. It is straightforward to deduce the symmetries

$$F_{l0}(\eta) = F^*_{-l0}(-\eta), \qquad Q^*_{l0}(\alpha) = Q_{l0}(-\alpha), \qquad Q_{-l0}(\alpha) = Q_{l0}(\alpha). \tag{85}$$

Let us now recast the integral equation (95) into a form with a Hermitian kernel by defining a modified transfer function and density transform (Zang 1976)

$$T_0(\alpha,\alpha') = \sqrt{\frac{K(\alpha,0)}{K(\alpha',0)}}\mathcal{S}_0(\alpha,\alpha') \qquad B(\alpha) = \sqrt{K(\alpha,0)}A(\alpha). \tag{86}$$

The integral equation (95) now becomes

$$\lambda B(\alpha) = \int_{-\infty}^{+\infty} d\alpha' B(\alpha')T_0(\alpha,\alpha'). \tag{87}$$

The value of this transformation is that $T_0(\alpha,\alpha')$ is Hermitian, viz

$$T^*_0(\alpha',\alpha) = T_0(\alpha,\alpha'). \tag{88}$$

The modified integral equation (87) is thus a homogeneous, linear Fredholm integral equation with a Hermitian kernel. It must therefore have real eigenvalues and orthogonal eigenfunctions (Tricomi 1985). This occurs because the mathematical eigenvalues have no dependence on pattern speed. In general, the mathematical eigenvalue λ is an analytic function of the complex frequency ω. Only for $m = 0$ is the frequency purely imaginary and the problem one-dimensional.

There is a further symmetry. We make the transformations $\alpha \to -\alpha$, $\alpha' \to -\alpha'$, $l \to -l$, so as to obtain $T_0^*(-\alpha, -\alpha')$. Using the symmetry properties of the Fourier coefficients and the angular momentum function (85) along with that of the Kalnajs gravity factor, we obtain the result

$$T_0^*(-\alpha, -\alpha') = T_0(\alpha, \alpha'). \tag{89}$$

This has the consequence that the eigenvalues are degenerate. If $B(\alpha)$ is an eigenvector with eigenvalue λ, then so is $B^*(-\alpha)$. To see this, we make the transformations $\alpha \to -\alpha$, $\alpha' \to -\alpha'$ in the modified integral equation (87), and take the complex conjugate. We obtain:

$$\lambda B^*(-\alpha) = -\int_{\infty}^{-\infty} d\alpha' B^*(-\alpha') T_0^*(-\alpha, -\alpha') = \int_{-\infty}^{+\infty} d\alpha' B^*(-\alpha') T_0(\alpha, \alpha'). \tag{90}$$

In other words, $B^*(-\alpha)$ also satisfies the integral equation (87). In terms of our original density transforms, $A(\alpha)$ and $A^*(-\alpha)$ are a degenerate pair with the same eigenvalue λ. This is just the anti-spiral theorem (Lynden-Bell & Ostriker 1967; Kalnajs 1971) for axisymmetric perturbations.

4 NUMERICAL METHODS

This section discusses the numerical algorithms required to find the normal modes. Sections 4.1 and 4.2 consider the evaluation of the Fourier coefficients and the transfer function respectively, whereas Section 4.3 presents the discretisation of the integral equation. Again, let us emphasise that the numerical method is adopted – with a little streamlining – from Zang (1976).

4.1 The Fourier Coefficient

The integrand in the definition of the Fourier coeffients (63) is periodic with period 2π in χ. We are free to define $\chi = 0$ to correspond to pericentre. This means that at the time $t = 0$, the star has radial coordinate $R = R_{\min}$. As $\tilde{X}$ is even, and $\tilde{Y}$ is odd, about $\chi = 0$, we can write

$$Q_{lm}(\alpha) = \frac{1}{\pi} \int_0^{\pi} \exp\left\{ (i\alpha - \tfrac{1}{2}) \tilde{X} \right\} \cos(m\tilde{Y} - l\chi)\, d\chi. \tag{91}$$

The equations of motion (16) are solved by fourth-order Runge-Kutta integration (Press *et al.* 1989, chap. 15) to obtain the stellar position as a function of time, and thus $\tilde{X}$ and $\tilde{Y}$ as a function of χ. The integration over χ is carried out by the midpoint method (Press *et al.* 1989, chap. 4), using n_ψ points in the midpoint integration and $2n_\psi$ in the Runge-Kutta. The problem is to choose n_ψ large enough to obtain excellent accuracy, while keeping it as small as possible in order to save time. Eccentric orbits need more work to obtain good accuracy, so, as suggested by Zang (1976), n_ψ is made to depend exponentially on $\tilde{U}$:

$$n_\psi = a_{\rm acc} \exp(b_{\rm acc} \tilde{U}). \tag{92}$$

Values of $a_{\rm acc} = 10$ and $b_{\rm acc} = 1.5$ usually worked well. With these values, the Fourier coefficient is obtained with around 6 s.f. accuracy for low eccentricity orbits ($\tilde{U} = 0.5$), but perhaps only 1 or 2 s.f. for high eccentricity orbits like ($\tilde{U} = 1.5$). The Fourier coefficients are generally smaller for higher values of the eccentric velocity. In the integrand for the transfer function, two Fourier coefficients are multiplied together at every eccentric velocity. The accuracy with which the transfer function is obtained is thus dominated by the accuracy of the Fourier coefficients at low eccentric velocities. This is useful, since the Fourier coefficients are costly to evaluate when the eccentric velocity is high. Fig. 7 shows the Fourier coefficient as a function of wavenumber, for two different eccentric velocities. It is shown only for positive wavenumber. Its behaviour for negative wavenumber is readily deduced from the symmetry property $Q_{lm}(\alpha) = Q_{lm}^*(-\alpha)$. We see that $\tilde{U}$ controls the amplitude and the frequency of oscillation of Q_{lm}. Fig. 8 compares Fourier coefficients at different radial harmonics. For high values of l, Q_{lm} remains close to zero until α is large; thereafter it oscillates with lower frequency. Logarithmic spiral components must be tightly-wound in order to excite responses at high radial harmonics.

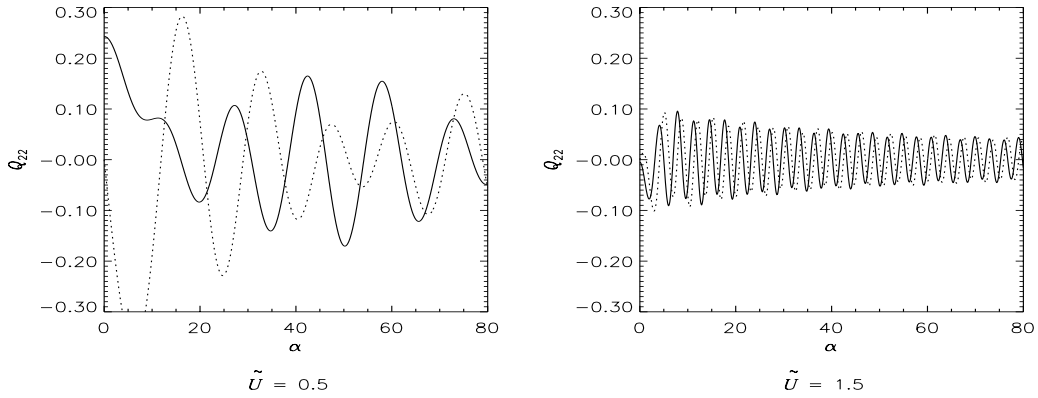

Figure 7. Graph of the Fourier coefficient Q_{22} plotted against wavenumber α. In the left-hand plot, $\tilde{U} = 0.5$; on the right, $\tilde{U} = 1.5$. In each case, the solid line is the real, and the dotted line the imaginary, part of Q_{22}. [Numerical details: $\beta = 0.25$, $m = 2$, $l = 2$; $a_{\rm acc} = 100$, $b_{\rm acc} = 2.5$.]

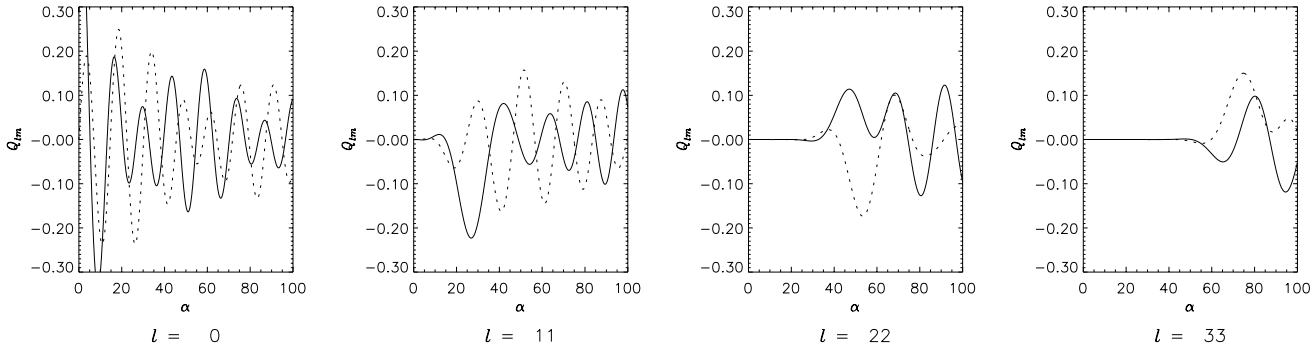

Figure 8. Graph of the Fourier coefficient Q_{lm} plotted against wavenumber α for four different radial harmonics l. In each case, the solid line is the real, and the dotted line the imaginary, part of Q_{lm}. [Numerical details: $\beta = 0.25$, $m = 2$, $\tilde{U} = 0.5$; $a_{\rm acc} = 100$, $b_{\rm acc} = 2.5$.]

4.2 The Transfer Function

The expression for the transfer function (78) involves a sum over radial harmonic l from $-\infty$ to $+\infty$. Fortunately, the magnitude of the terms in this sum decreases sharply with $|l|$. Negative values of l decrease their contribution faster than positive l. A good approximation is given by summing from $l = l_{\rm min}$ to $l = l_{\rm max}$, where $l_{\rm min}$ is negative and $|l_{\rm min}|$ is less than $l_{\rm max}$. Values of $l_{\rm min} = -20$, $l_{\rm max} = 30$ usually worked well. The transfer function also contains an integral over eccentric velocity $\tilde{U}$, which adds up orbits of all possible shapes. The equivalent expression for the Toomre-Zang disk (80) contains a Gaussian factor $\exp(-\frac{1}{2}\tilde{U}^2/\tilde{\sigma}_u^2)$. This prompted Zang (1976) to use Gauss-Laguerre quadrature to evaluate $\mathcal{S}_m$. The fundamental formula is

$$\int_0^\infty f(x)e^{-x}dx \approx \sum_{i=1}^{n_{GL}} w_i f(x_i), \tag{93}$$

where $f(x)$ is a smooth polynomial-like function. The weights w_i and abscissae x_i are well-known (see Abramowitz & Stegun 1989; Press *et al.* 1989, chap. 4). Zang (1976) found it preferable to reduce the dispersion of the Gaussian in this expression, replacing it with $\tilde{\sigma}_n = f_\sigma \tilde{\sigma}_u$, where the fraction f_σ is around 80%. This concentrates attention on the lower values of $\tilde{U}$, where the integrand is larger. For the power-law disks, the distribution of radial velocities at any spot is similar – but not exactly equal to – a Gaussian with dispersion $\tilde{\sigma}_u$. This suggests that Gauss-Laguerre quadrature may still work well. Although our integrand is not directly of form (93), it is readily made so. The limits on our integral are zero and infinity for negative β. For positive β, the upper limit is $\tilde{U} = (2/\beta - 1)^{1/2}$. At least for the models of most interest in galactic astronomy ($|\beta| \lesssim 0.5$), this distinction is in practice unimportant, since the integrand has fallen to negligibly small values well before this limit on the eccentric velocity.

Let $\mathcal{I}_U$ be the integrand in $\mathcal{S}_m$ when the integration is carried out over $\tilde{U}$, so $\mathcal{S}_m(\alpha, \alpha') \propto \int_0^\infty \mathcal{I}_U d\tilde{U}$. We then have

$$\mathcal{I}_V = \mathcal{I}_U \frac{\tilde{\sigma}_n^2}{\tilde{U}} \exp\left(\frac{\tilde{U}^2}{2\tilde{\sigma}_n^2}\right), \tag{94}$$

where $\mathcal{S}_m(\alpha,\alpha') \propto \int_0^\infty \mathcal{I}_V e^{-V} dV$ and $V = \frac{1}{2}\tilde{U}^2/\tilde{\sigma}_n^2$. The reliability of Gauss-Laguerre quadrature was tested against the extended midpoint method (Press *et al.* 1989, eq. (4.1.19)). These comparisons (Read 1997) indicate that Gauss-Laguerre quadrature is a remarkably efficient way of performing the integral. Excellent six significant figure accuracy is obtained with a handful of function evaluations.

4.3 Computational Solution of the Integral Equation

Given that the kernel of the integral equation can be evaluated to high accuracy, we now need to devise a method for its numerical solution. We ultimately seek self-consistent solutions, for which $A_{\rm res}(\alpha) = A_{\rm imp}(\alpha)$. However, as Zang (1976) already noted, the first step is to consider the more general problem for which the response density is a complex multiple of the imposed density, i.e., $A_{\rm res}(\alpha) = \lambda A_{\rm imp}(\alpha)$. This casts the integral equation (57) into the form

$$\lambda A(\alpha) = \int_{-\infty}^{+\infty} d\alpha' A(\alpha')\, \mathcal{S}_m(\alpha,\alpha'), \tag{95}$$

where we have dropped the subscripts on A. We refer to λ as the mathematical eigenvalue. Of course, only the instance when λ is unity carries the physical significance of a mode. The advantage of this mathematical artifice is that the integral equation (95) is in the standard form of a homogeneous, linear, Fredholm equation of the second kind (see e.g. Courant & Hilbert 1953; Delves & Mohamed 1985). For a given value of λ, such an equation normally admits only the trivial solution, $A(\alpha) \equiv 0$. The values of λ for which non-trivial solutions exist are the eigenvalues of the equation. We seek an iterative scheme which drives the eigenvalue to unity, thus providing a self-consistent mode. There is a close analogy between linear algebraic equations and linear integral equations. The former define relations between vectors in a finite-dimensional vector space, the latter define relations between functions in an infinite-dimensional vector space (technically, a Banach space). This analogy can be made explicit by applying a quadrature rule to the integration in (95) to obtain

$$\lambda A(\alpha_j) = \sum_i w_i A(\alpha_i)\, \mathcal{S}_m(\alpha_j,\alpha_i), \tag{96}$$

where w_i are some appropriate weights. This general approach is called the Nystrom method (Delves & Mohamed 1985). It evidently reduces the solution of an integral equation to the solution of an algebraic eigenvalue problem. The latter is a classic and well-studied area of numerical analysis, for which many tried and tested techniques are available.

Much of the skill in the numerical solution of integral equations comes from the choice of quadrature rules and weights. Zang (1976) devised an elegant method based on locally approximating the kernel and the response by Lagrangian interpolating polynomials. This is naturally adapted to the instance when the kernel varies on a much smaller scale than the solution. We follow this method, but we did not find Zang's splitting of the kernel of the integral equation into Hermitian and Volterra parts to be needed. First, to obtain smoother functions, the Kalnajs gravity factor is extracted by defining

$$\mathcal{S}_m(\alpha,\alpha') = K(\alpha',m)\,\tilde{\mathcal{S}}_m(\alpha,\alpha'), \qquad A(\alpha) = \frac{\tilde{A}(\alpha)}{K(\alpha,m)}. \tag{97}$$

The eigenvalue equation now becomes

$$\lambda \tilde{A}(\alpha) = K(\alpha,m) \int_{-\infty}^{+\infty} d\alpha' \tilde{A}(\alpha')\, \tilde{\mathcal{S}}_m(\alpha,\alpha'). \tag{98}$$

Let us introduce a finite grid of points in wavenumber space, α_r. If we need to know the value of $\tilde{A}$ or $\tilde{\mathcal{S}}_m$ at a value of α intermediate between the gridpoints α_r and α_{r+1}, we interpolate over the eight gridpoints from α_{r-3} to α_{r+4}. For 8 equally-spaced points $\Delta\alpha$ apart, Lagrange's classic formula for the interpolating polynomial $P(\alpha)$ through N points $f(\alpha_k)$ (Press *et al.* 1989, chap. 3) becomes

$$P(\alpha) = \prod_{i=1}^{8} (\alpha - \alpha_{r+i-4}) \sum_{k=-3}^{4} \frac{(-1)^k}{(3+k)!(4-k)!} \frac{f(\alpha_{r+k})}{(\Delta\alpha)^7(\alpha - \alpha_r - k\Delta\alpha)}. \tag{99}$$

Defining $x = (\alpha - \alpha_r)/\Delta\alpha$, this becomes

$$P(\alpha) = \prod_{i=1}^{8} (x+4-i) \sum_{k=-3}^{4} (-1)^k \frac{f(\alpha_{r+k})}{(3+k)!(4-k)!(x-k)} = \sum_{k=-3}^{4} L_k[x] f(\alpha_{r+k}), \tag{100}$$

where

$$L_k[x] = (-1)^k \frac{\prod_{i=1}^{8}(x+4-i)}{(3+k)!(4-k)!(x-k)}. \tag{101}$$

Then the interpolated approximations to the response and the transfer function are (cf. Zang 1976, app. D)

$$\tilde{A}(\alpha') \approx \sum_{k=-3}^{4} L_k[x']\tilde{A}(\alpha_{r+k}), \qquad \tilde{\mathcal{S}}_m(\alpha,\alpha') \approx \sum_{k=-3}^{4} L_k[x']\tilde{\mathcal{S}}_m(\alpha,\alpha_{r+k}), \tag{102}$$

where $x' = (\alpha' - \alpha_r)/\Delta\alpha$. The infinite range in the integral equation (95) is a kind of singularity. Truncation of the wavenumber range at large finite values is the simplest but most brutal way of handling the singularity. In practice, we found this to be surprisingly effective. Wavenumber space is approximated by a finite grid with n points along each side. We choose n, and the grid-point spacing $\Delta\alpha$, so as to obtain a sufficiently accurate solution of the integral equation (57). The finite size of the grid means that we encounter problems when evaluating $\tilde{A}_{\rm imp}$ and $\tilde{\mathcal{S}}_m$ for values of α near the edges of the grid. We are interpolating over eight points, so we need data from α_{-2} to α_{n+3}. We deal with this problem by simply assuming that our function is zero outside the grid. This is acceptable provided the grid is large enough. Then the values of the kernel at the missing interpolation points are negligibly small. This procedure is justified empirically by the demonstration that the mathematical eigenvalue converges to a value independent of grid size (Read 1997).

Substituting the Lagrange-interpolated approximations for $\tilde{A}_{\rm imp}$ and $\tilde{\mathcal{S}}_m$ (102) into the modified integral equation (98), we obtain

$$\lambda\tilde{A}(\alpha) = K(\alpha,m)\sum_{i=-3}^{4}\sum_{k=-3}^{4}\int_{\alpha_1}^{\alpha_n} d\alpha' L_i\left[\frac{\alpha'-\alpha_r}{\Delta\alpha}\right] L_k\left[\frac{\alpha'-\alpha_r}{\Delta\alpha}\right]\tilde{A}(\alpha'_{r+i})\tilde{\mathcal{S}}_m(\alpha,\alpha'_{r+k}). \tag{103}$$

Of course, the integration over wavenumber now runs from $\alpha = \alpha_1$ to α_n, instead of from $\alpha = -\infty$ to ∞. We break this integration into n portions of $\Delta\alpha$.

$$\lambda\tilde{A}(\alpha) = K(\alpha,m)\sum_{r=1}^{n}\sum_{i=-3}^{4}\sum_{k=-3}^{4}\int_{\alpha_r}^{\alpha_r+\Delta\alpha} d\alpha' L_i\left[\frac{\alpha'-\alpha_r}{\Delta\alpha}\right] L_k\left[\frac{\alpha'-\alpha_r}{\Delta\alpha}\right]\tilde{A}(\alpha'_{r+i})\tilde{\mathcal{S}}_m(\alpha,\alpha'_{r+k}). \tag{104}$$

Then, changing variables to $x' = (\alpha' - \alpha_r)/\Delta\alpha$, we obtain

$$\lambda\tilde{A}(\alpha) = K(\alpha,m)\sum_{r=1}^{n}\sum_{i=-3}^{4}\sum_{k=-3}^{4}\tilde{A}(\alpha_{r+i})\tilde{\mathcal{S}}_m(\alpha,\alpha_{r+k})\Delta\alpha\int_0^1 dx' L_i[x']L_k[x']. \tag{105}$$

Let us define the weighting coefficients C_{ik} by (cf. Zang (1976), app. D)

$$C_{ik} = \Delta\alpha\int_0^1 dx L_i[x]L_k[x]. \tag{106}$$

Although there appear to be 64 C_{ik}, only 20 of them are independent, because of the symmetry properties $C_{ik} \equiv C_{ki}$, and $C_{ik} \equiv C_{(1-i)(1-k)}$. The weighting coefficients are easily evaluated using the midpoint method given in Press *et al.* (1989, chap. 4). They are tabulated in Read (1997). Equation (103) can now be written as:

$$\lambda\tilde{A}(\alpha_j) = K(\alpha_j,m)\sum_{r=1}^{n}\sum_{i=-3}^{4}\sum_{k=-3}^{4} C_{ik}\tilde{\mathcal{S}}_m(\alpha_j,\alpha_{r+k})\tilde{A}(\alpha_{r+i}) \tag{107}$$

Terms in this multiple sum for which $r+i$ is less than 1 or greater than n contribute nothing. We can thus write the above equation in terms of a single sum from α_1 to α_n, and collect the weighting coefficients C_{ik}, smoothed transfer function $\tilde{\mathcal{S}}_m$ and density profile $\tilde{A}$ together into a single quantity $\mathbf{S}$.

$$\lambda\tilde{A}(\alpha_j) = \sum_{s=1}^{n} S_{js}\tilde{A}(\alpha_s). \tag{108}$$

This is of course just a matrix equation for the mathematical eigenvalue λ. If there is an eigenvalue of the matrix

S equal to unity, then the corresponding eigenvector **A** gives us a self-consistent mode, i.e. a self-sustaining density perturbation. S_{js} cannot be simply expressed in terms of C_{ik}, $\tilde{\mathcal{S}}_m$ and $\tilde{A}$. But we see that it represents the total coefficient of $\tilde{A}(\alpha_s)$ in eq. (107).

Having obtained the matrix S_{js}, it is reasonably straightforward to find its eigenvalues using the eigensystem package (*EISPACK*) developed by Smith *et al.* (1972). This returns the eigenvalues of a matrix and, optionally, the corresponding eigenvectors. The power method can also be used to provide an independent check on the largest eigenvalue. This relies on repeated application of the matrix **S** to a test vector **t** (Ralston & Rabinowitz 1978, chap. 8, sec. 7). Probably the most important factor in achieving excellent accuracy in the eigenvalues is the size and fineness of the grid. The range of the grid, $(n-1)\Delta\alpha$, typically needs to be around 50 in order for the mathematical eigenvalue to be accurate to 6 s.f. A grid-spacing of $\Delta\alpha = 0.2$ is usually sufficient. However, suitable values necessarily depend to some extent on the form of the mode. For instance, for high azimuthal harmonics, the modes tend to be tightly-wrapped, requiring a more extensive grid.

Having established that the mathematical eigenvalue can be found to good accuracy, let us consider how to locate the unit eigenvalues which correspond to self-consistent modes. We are investigating modes of a given azimuthal symmetry in a disk with given density profile. This means that m, β, N, M and $\tilde{L}_{\rm c}$ are held fixed. It leaves us free to adjust γ, s and $\Omega_{\rm p}$. A disk at a given temperature, if it admits a mode at all, generally does so only for a particular growth rate and pattern speed. We therefore hold γ fixed, and adjust s and $\Omega_{\rm p}$ until a mode is found. This is in fact a search for the root of the equation $\lambda = 1$ in only one dimension, since the mathematical eigenvalue λ is an analytic function of the complex frequency $\omega = m\Omega_{\rm p} + is$. The Newton-Raphson method is extremely effective at locating such roots. When the disk is sufficiently hot, it is generally completely stable. As the disk is cooled, instabilities set in through the marginal modes, for which the growth rate s is zero. We are therefore often interested in the marginally stable modes. To find these, s is set to some vanishingly small value, and a two-dimensional search is performed for the critical pattern speed $\Omega_{\rm p}$ and temperature γ using the Newton-Raphson method in two dimensions.

5 CONCLUSIONS

This paper has set up the machinery for an investigation into the large-scale, global, modes of the power-law disks. The Fredholm integral equation for the normal modes has been derived. This is done by linearising the collisionless Boltzmann equation to find the response density corresponding to any imposed density and potential. The normal modes are given by equating the imposed density to the response density. This scheme is implemented in Fourier space, so that the Fredholm integral equation relates the transform of the imposed density to the transform of the response density. Numerical strategies are given to discretise the integral equation to yield a matrix equation. This requires some care as the kernel of the integral equation is either singular (as in the case of the self-consistent disk) or almost so (the cut-out disks). The problem of locating the normal modes is thus reduced to an algebraic eigenvalue problem, for which a wealth of standard techniques are available. The crucial simplification underlying the analysis is that the force law describing the gravity field of the galactic disk is scale-free. It is this that ensures that orbits passing through any one spot in the disk are simply scaled copies of the orbits passing through any other spot. When the orbits are forced by a scale-free logarithmic spiral perturbation, the response of all orbits of the same eccentricity can be computed at the same time. It only remains to add up the contributions at every eccentricity. For a disk with an arbitrary force law, such simplification is not possible.

Let us again emphasise that nearly all the computational techniques required to study the stability of the power-law disks were developed by Zang (1976) in his pioneering study of the disk with a completely flat rotation curve. Our contribution consists *only* of deriving the extensions to study the complete family of scale-free power-law disks. This paper has discussed just the algorithms – the aim has been to present all the mathematical and computational details for reference here. The following paper in this issue of *Monthly Notices* implements the machinery discussed here to provide a complete description of the spiral modes of the self-consistent and cut-out power-law disks. A fast computer code is developed which gives the growth rates and pattern speeds of the normal modes for any power-law disk in a matter of minutes when run on a modern workstation.

NWE thanks Alar Toomre for much generous and helpful advice on how to extend the analysis in Zang's thesis to the family of power-law disks. NWE is also grateful to the trustees of the Lindemann Fellowship for an award which enabled him to spend the year of 1994 at the Massachusetts Institute of Technology. He is supported by the Royal Society. JCAR thanks the Particle Physics and Astronomy Research Council for a research studentship.

REFERENCES

Binney J. & Tremaine S., 1987, Galactic Dynamics, Princeton University Press, Princeton
Bisnovatyi-Kogan E., 1976, SvA Lett, 1, 177
Casertano S. & van Gorkom J. H., 1991, AJ, 101, 1231
Delves L. M. & Mohamed J. L., 1985, Computational Methods for Integral Equations, Cambridge University Press, Cambridge
Earn D. J. D., 1993, Ph.D. thesis, Cambridge University, Cambridge
Earn D. J. D. & Sellwood J. A., 1995, ApJ, 451, 533
Evans N. W., 1994, MNRAS, 267, 333
Evans N. W. & Collett J. L., 1993, MNRAS, 264, 353
Jeans J. H., 1919, Problems of Cosmogony & Stellar Dynamics, Cambridge University Press, Cambridge
Kalnajs A. J., 1965, Ph.D. thesis, Harvard University, Cambridge, Massachusetts
Kalnajs A. J., 1971, ApJ, 166, 275
Kalnajs A. J., 1972, ApJ, 175, 63
Lemos J. P. S., Kalnajs A. J., & Lynden-Bell D., 1991, ApJ, 375, 484
Lynden-Bell D. & Ostriker J. P., 1967, MNRAS, 136, 101
Merritt D. & Sellwood J. A., 1994, ApJ, 425, 551
Mestel L., 1963, MNRAS, 126, 553
Mihalas D. & Binney J. J., 1987, Galactic Astronomy, W. H. Freeman, San Francisco
Ostriker J. P. & Peebles P. J. E., 1973, ApJ, 186, 467
Palmer P. L. & Papaloizou J., 1990, MNRAS, 243, 263
Press W., Flannery B., Teukolsky S., & Vetterling W., 1989, Numerical Recipes: the art of scientific computing, Cambridge University Press, Cambridge
Prudnikov A. P., Brychkov Y. A., & Mavichev O., 1986, Integrals and Series, vol. 1, Gordon and Breach, New York
Ralston A. & Rabinowitz P., 1978, A First Course in Numerical Analysis, McGraw-Hill, New York
Read J. C. A., 1997, Ph.D. thesis, Oxford University, Oxford
Rubin V. C., W. Kent Ford J., & Thonnard N., 1978, ApJ, 225, L107
Schmitz F. & Ebert R., 1987, A&A, 181, 41
Sellwood J. A. & Athanassoula E., 1986, MNRAS, 221, 195
Smith B. T., Boyle J. M., Dongarra J. J., Garbow B. S., Ikebe Y., Klema V. C., & Moler C. B., 1972, Lecture Notes in Computer Science, Vol. 6, Springer-Verlag, Berlin-Heidelberg-New York, 2nd edition
Snow C., 1952, Hypergeometric and Legendre Functions with Applications to the Integral Equations of Potential Theory, National Bureau of Standards, Washington
Toomre A., 1977, ARAA, 15, 437
Toomre A., 1981, in S. M. Fall & D. Lynden-Bell (eds.), The Structure and Evolution of Normal Galaxies, p. 111, Cambridge University Press, Cambridge
Tricomi F., 1985, Integral Equations, Dover, New York
Zang T. A., 1976, Ph.D. thesis, Massachusetts Institute of Technology, Cambridge, Massachusetts

APPENDIX A: SINGLE-ECCENTRICITY DISTRIBUTION FUNCTIONS

In the main body of the paper, we have used stellar distribution functions for the power-law disks that are built from powers of energy and angular momentum. Many other equilibrium distribution functions are possible. In this Appendix, we consider disks in which all the stars have the same shape of orbit, characterised by an eccentric velocity $U = U_r$. Mathematically, we look for distribution functions of the form

$$f_{\rm s} = F(R_{\rm H})\delta(U - U_r). \tag{A1}$$

The surface density is

$$\Sigma_{\rm eq} = \Sigma_0 \left(\frac{R_0}{R}\right)^{1+\beta} = \iint f_{\rm s}(u,v)\,du\,dv. \tag{A2}$$

We transform this to an integral over U and R_H, using the Jacobian

$$du\,dv = dU\,dR_H \left(1 - \frac{\beta}{2}\right) \frac{v_\beta}{R} \left(\frac{R_0}{R_H}\right)^{\beta/2} \frac{\tilde{U}}{\sqrt{\tilde{U}^2 + 1 - \tilde{R}^{-2} + \frac{2}{\beta}(\tilde{R}^{-\beta} - 1)}}, \tag{A3}$$

and substitute our assumed distribution function

$$\Sigma_0 \left(\frac{R_0}{R}\right)^{1+\beta} = \left(1 - \frac{\beta}{2}\right) \frac{v_\beta}{R} \iint \left(\frac{R_0}{R_H}\right)^{\beta/2} \frac{\tilde{U}\,F(R_{\rm H})\,\delta(U - U_r)\,dU\,dR_H}{\sqrt{\tilde{U}^2 + 1 - \tilde{R}^{-2} + \frac{2}{\beta}(\tilde{R}^{\beta} - 1)}}. \tag{A4}$$

We integrate over U, and then transform the integral over $R_{\rm H}$ to one over $\tilde{R} = R/R_H$:

$$\Sigma_0 \left(\frac{R_0}{R}\right)^{1+\beta/2} = \left(1-\frac{\beta}{2}\right) 2 v_\beta \tilde{U}_r \int_{\tilde{R}_{\rm min}}^{\tilde{R}_{\rm max}} \frac{\tilde{R}^{\beta/2} F\left(R/\tilde{R}\right)\, d\tilde{R}}{\tilde{R}^2 \sqrt{\tilde{U}_r^2 + 1 - \tilde{R}^{-2} + \frac{2}{\beta}(\tilde{R}^\beta - 1)}}, \tag{A5}$$

where $\tilde{U}_r$ is the value of U_r in dimensionless units. Looking at the powers of R, we can guess at a solution of this integral equation, namely $F(R/\tilde{R}) = k(\tilde{R}/R)^{1+\beta/2}$. Substituting this into (A5), and remembering the definition of the auxiliary integral $\mathcal{J}_n(\tilde{U})$ (18), we can solve for k and obtain

$$k = \frac{\Sigma_0 R_0^{1+\beta/2}}{(1-\frac{\beta}{2}) v_\beta \tilde{U}_r \mathcal{J}_{1-\beta}(\tilde{U}_r)} = \frac{\Sigma_0 R_0^{1+\beta}}{\left(1-\frac{\beta}{2}\right) R_{\rm H}^{\beta/2} U_r \mathcal{J}_{1-\beta}(\tilde{U}_r)}. \tag{A6}$$

The distribution function is then

$$f_{\rm s}(U, R_{\rm H}) = \frac{\Sigma_0 R_0^{1+\beta}}{\left(1-\frac{\beta}{2}\right) U_r \mathcal{J}_{1-\beta}(\tilde{U}_r)} \frac{\delta(U-U_r)}{R_{\rm H}^{1+\beta}}. \tag{A7}$$

This expression is valid for $\beta = 0$, in which case the appropriate form for the auxiliary integral $\mathcal{J}_1$ (19) must be used.

All the stars in this disk have orbits of the same shape, but different size. Each star sweeps out an annulus as it orbits. The relative width of this annulus depends on the eccentric velocity U_r, but the overall size of the annulus depends on $R_{\rm H}$. It is easy to imagine that if we add up annuli with a variety of $R_{\rm H}$ in suitable proportions, we could recover the surface density of the equilibrium disk; and this is what the distribution function (A7) does. It seems intuitively right that the number of annuli needed falls off with $R_{\rm H}$ at the same rate as the surface density falls off with R. Similarly, we can see why the total number of annuli depends inversely on eccentric velocity U_r: for high U_r, the annuli are very wide, and few are needed; for low U_r, the converse is true.

APPENDIX B: REFERENCE TABLE OF DIMENSIONLESS QUANTITIES

	Quantity	For the Toomre-Zang disk	For the general power-law disk
$\tilde{R}_{\rm H}$	Home radius	$\tilde{R}_H = R_{\rm H}/R_0$	$\tilde{R}_H = R_{\rm H}/R_0$
$\tilde{t}$	Time	$\tilde{t} = \frac{v_0}{R_{\rm H}} t$	$\tilde{t} = \frac{v_\beta}{R_{\rm H}} \tilde{R}_H^{-\beta/2} t$
$\tilde{u}$	Radial velocity	$\tilde{u} = \frac{d\tilde{R}}{d\tilde{t}} = \frac{u}{v_0}$	$\tilde{u} = \frac{d\tilde{R}}{d\tilde{t}} = \frac{u}{v_\beta} \tilde{R}_H^{\beta/2}$
$\tilde{v}$	Tangential velocity	$\tilde{v} = \frac{\tilde{R} d\theta}{d\tilde{t}} = \frac{v}{v_0}$ $\tilde{v} = \tilde{R}^{-1}$	$\tilde{v} = \frac{\tilde{R} d\theta}{d\tilde{t}} = \frac{v}{v_\beta} \tilde{R}_H^{\beta/2}$ $\tilde{v} = \tilde{R}^{-1}$
$\tilde{E}$	Energy	$\tilde{E} = \frac{E}{v_0^2}$; $\tilde{E} = \frac{1}{2}\left(\tilde{u}^2 + \tilde{v}^2\right) - \ln \frac{R_0}{R}$	$\tilde{E} = \frac{E}{v_\beta^2} \tilde{R}_H^\beta$; $\tilde{E} = \frac{1}{2}\left(\tilde{u}^2 + \tilde{v}^2\right) - \frac{1}{\beta \tilde{R}^\beta}$
$\tilde{L}_z$	Angular momentum	$\tilde{L}_z = \frac{L_z}{R_0 v_0} = \tilde{R}$	$\tilde{L}_z = \frac{L_z}{R_0 v_\beta} = \tilde{R}^{1-\beta/2}$
$\tilde{U}$	Eccentric velocity	$\tilde{U} = \frac{U}{v_0}$	$\tilde{U} = \frac{U}{v_\beta} \tilde{R}_H^{\beta/2}$
		$\tilde{U}^2 = \tilde{u}^2 - 1 + \tilde{R}^{-2} + 2\ln \tilde{R}$	$\tilde{U}^2 = \tilde{u}^2 - 1 + \tilde{R}^{-2} - \frac{2}{\beta}\left(\tilde{R}^{-\beta} - 1\right)$
$\mathcal{J}_n$	Auxiliary integral	$\mathcal{J}_n = \int_{\tilde{R}_{\rm min}}^{\tilde{R}_{\rm max}} \frac{2 d\tilde{R}}{\tilde{R}^n \left(\tilde{U}^2 + 1 - \tilde{R}^{-2} - 2\ln \tilde{R}\right)^{\frac{1}{2}}}$	$\mathcal{J}_n = \int_{\tilde{R}_{\rm min}}^{\tilde{R}_{\rm max}} \frac{2 d\tilde{R}}{\tilde{R}^n \left(\tilde{U}^2 + 1 - \tilde{R}^{-2} + \frac{2}{\beta}\left(\tilde{R}^{-\beta} - 1\right)\right)^{\frac{1}{2}}}$
$\tilde{\kappa}$	Radial frequency	$\tilde{\kappa} = \frac{R_{\rm H}}{v_0} \kappa = \frac{2\pi}{\mathcal{J}_0}$	$\tilde{\kappa} = \frac{R_{\rm H}}{v_\beta} \tilde{R}_H^{\beta/2} \kappa = \frac{2\pi}{\mathcal{J}_0}$
$\tilde{\Omega}$	Angular frequency	$\tilde{\Omega} = \frac{R_{\rm H}}{v_0} \Omega = \frac{\mathcal{J}_2}{\mathcal{J}_0}$	$\tilde{\Omega} = \frac{R_{\rm H}}{v_\beta} \tilde{R}_H^{\beta/2} \Omega = \frac{\mathcal{J}_2}{\mathcal{J}_0}$
$\tilde{\kappa}_0$	Epicyclic frequency	$\tilde{\kappa}_0 = \sqrt{2}$	$\tilde{\kappa}_0 = \sqrt{2-\beta}$
$\tilde{\Omega}_0$	Circular frequency	$\tilde{\Omega}_0 = 1$	$\tilde{\Omega}_0 = 1$
χ	Orbital phase	$\chi = \kappa t = \tilde{\kappa} \tilde{t}$	$\chi = \kappa t = \tilde{\kappa} \tilde{t}$
$\tilde{Y}$	Angular deviation	$\tilde{Y} = \theta - \Omega t = \theta - \tilde{\Omega} \tilde{t}$	$\tilde{Y} = \theta - \Omega t = \theta - \tilde{\Omega} \tilde{t}$
$\tilde{x}$	Logarithmic radius	$\tilde{x} = \ln\left(\frac{R}{R_0}\right)$	$\tilde{x} = \ln\left(\frac{R}{R_0}\right)$
$\tilde{X}$	Scaled logarithmic radius	$\tilde{X} = \ln\left(\frac{R}{R_{\rm H}}\right) = \ln \tilde{R}$	$\tilde{X} = \ln\left(\frac{R}{R_{\rm H}}\right) = \ln \tilde{R}$
$\tilde{\sigma}_u$	Radial velocity dispersion	$\tilde{\sigma}_u^2 = \frac{1}{1+\gamma}$	$\tilde{\sigma}_u^2 = \frac{1}{1+\gamma+2\beta}$
γ	Anisotropy parameter	$\gamma = \frac{1}{\tilde{\sigma}_u^2} - 1$	$\gamma = \frac{1}{\tilde{\sigma}_u^2} - 1 - 2\beta$

APPENDIX C: THE ANGULAR MOMENTUM FUNCTION

In this Appendix, we derive the forms of the angular momentum function by explicitly performing the contour integration over angular momentum $\tilde{L}_z$. Let us recall the angular momentum function is

$$F_{lm} = \frac{1}{2\pi}\int_0^\infty \frac{e^{-i\eta\frac{2}{2-\beta}\ln\tilde{L}_z}}{l\tilde{\kappa}+m\tilde{\Omega}-\tilde{\omega}\tilde{L}_z^{\frac{2+\beta}{2-\beta}}}\left[\left\{(l\tilde{\kappa}+m\tilde{\Omega})\left|\frac{2+2\gamma-\beta\gamma}{\beta\tilde{U}^2+\beta-2}\right|-\gamma m\right\}\tilde{H}-m\tilde{L}_z\frac{d\tilde{H}}{d\tilde{L}_z}\right]\frac{d\tilde{L}_z}{\tilde{L}_z}.$$

The integration is carried out over the variable h defined by

$$h=\frac{2+\beta}{2-\beta}\ln\tilde{L}_z, \qquad \tilde{H}(\tilde{L}_z)=\mathcal{H}(h). \tag{C1}$$

It is performed for three different cut-out factors, namely the self-consistent disk, the inner cut-out disk and the doubly cut-out disk (all defined in eq. (41)). We proceed by splitting up the integral into two parts:

$$F_{lm}(\eta)=\left\{(l\tilde{\kappa}+m\tilde{\Omega})\left|\frac{2+2\gamma-\beta\gamma}{\beta\tilde{U}^2+\beta-2}\right|-\gamma m\right\}J_1-mJ_2, \tag{C2}$$

where

$$J_1(\beta,\eta,\tilde{L}_c)=\frac{1}{2\pi}\frac{2-\beta}{2+\beta}\int_{-\infty}^{\infty}\frac{e^{-i\eta\frac{2}{2+\beta}h}}{l\tilde{\kappa}+m\tilde{\Omega}-\tilde{\omega}e^h}\mathcal{H}(h)dh, \qquad J_2(\beta,\eta,\tilde{L}_c)=\frac{1}{2\pi}\int_{-\infty}^{\infty}\frac{e^{-i\eta\frac{2}{2+\beta}h}}{l\tilde{\kappa}+m\tilde{\Omega}-\tilde{\omega}e^h}\frac{d\mathcal{H}}{dh}dh. \tag{C3}$$

We need evaluate these only for the case $\beta=0$, since the general integrals are related to the $\beta=0$ integrals as

$$J_1(\beta,\eta,\tilde{L}_c)=\frac{2-\beta}{2+\beta}J_1\left(0,\hat{\eta},\tilde{L}_c^{\frac{2+\beta}{2-\beta}}\right), \qquad J_2(\beta,\eta,\tilde{L}_c)=J_2\left(0,\hat{\eta},\tilde{L}_c^{\frac{2+\beta}{2-\beta}}\right), \qquad \text{with } \hat{\eta}\equiv\eta\times\frac{2}{2+\beta}. \tag{C4}$$

$\tilde{L}_c$ has been included as an argument, although clearly this is only relevant to the doubly cut-out disk. We suppress the third argument unless needed.

C1 The self-consistent disk

Here

$$J_1(0,\eta)=\frac{1}{2\pi}\int_{-\infty}^{\infty}\frac{e^{-i\eta h}}{l\tilde{\kappa}+m\tilde{\Omega}-\tilde{\omega}e^h}dh, \qquad J_2(0,\eta)=0. \tag{C5}$$

We first consider the case $\omega\neq 0$. J_1 may be evaluated by contour integration. The integrand has poles when $h_n=\ln[(l\tilde{\kappa}+m\tilde{\Omega})/\tilde{\omega}]+2ni\pi$, where n is an integer. The poles occur at intervals along a line parallel to the imaginary axis. Note that $\tilde{\omega}$ is not in general real ($\omega=m\Omega_p+is$), so that the poles are displaced from the lines $h=2ni\pi$. We evaluate the integral

$$\frac{1}{2\pi}\oint\frac{e^{\lambda h}e^{-i\eta h}}{l\tilde{\kappa}+m\tilde{\Omega}-\tilde{\omega}e^h}dh, \tag{C6}$$

around a rectangular contour as shown in the left-hand plot of fig. C1, with long sides at $h=0$, $h=2i\pi$, and short edges at $\pm L$, enclosing the pole at $h=\ln[(l\tilde{\kappa}+m\tilde{\Omega})/\tilde{\omega}]$. Here the logarithm denotes the principal value, i.e. the imaginary part lies between 0 and 2π. Then

$$\begin{aligned}&\frac{1}{2\pi}\int_{-L}^{L}\frac{e^{\lambda h}e^{-i\eta h}dh}{l\tilde{\kappa}+m\tilde{\Omega}-\tilde{\omega}e^h}-\frac{e^{2i\pi\lambda}e^{2\pi\eta}}{2\pi}\int_{-L}^{L}\frac{e^{\lambda h}e^{-i\eta h}dh}{l\tilde{\kappa}+m\tilde{\Omega}-\tilde{\omega}e^h}+\frac{1}{2\pi}\int_0^{2\pi}\frac{e^{\lambda L}e^{y\eta}e^{i\lambda y}e^{-i\eta L}dh}{l\tilde{\kappa}+m\tilde{\Omega}-\tilde{\omega}e^{iy}e^L}\\&-\frac{1}{2\pi}\int_0^{2\pi}\frac{e^{-\lambda L}e^{y\eta}e^{i\lambda y}e^{i\eta L}dh}{l\tilde{\kappa}+m\tilde{\Omega}-\tilde{\omega}e^{iy}e^{-L}}=-\frac{i}{l\tilde{\kappa}+m\tilde{\Omega}}e^{\lambda\ln\frac{l\tilde{\kappa}+m\tilde{\Omega}}{\tilde{\omega}}}e^{-\eta\ln\frac{l\tilde{\kappa}+m\tilde{\Omega}}{\tilde{\omega}}}\end{aligned} \tag{C7}$$

Taking $L\to\infty$, and then $\lambda\to 0$, we obtain the result

$$J_1(0,\eta)=-\frac{ie^{-i\eta\ln\frac{l\tilde{\kappa}+m\tilde{\Omega}}{\tilde{\omega}}}}{(l\tilde{\kappa}+m\tilde{\Omega})(1-e^{2\pi\eta})}. \tag{C8}$$

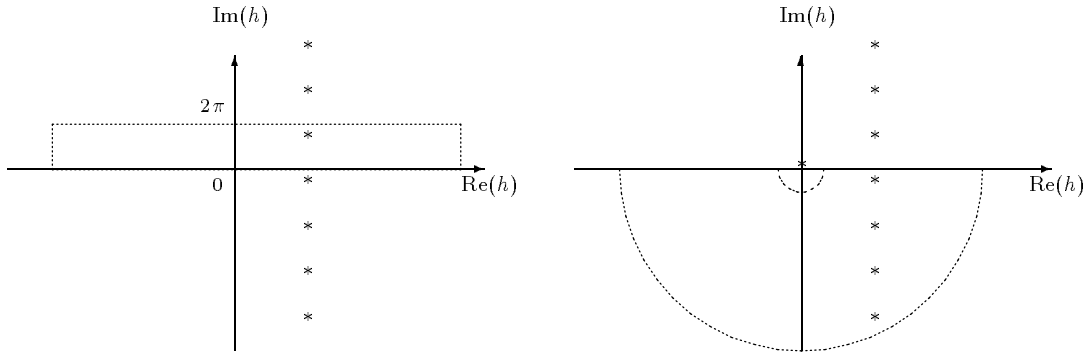

Figure C1. Contours and poles for the self-consistent disk. The left-hand plot shows the contour used for $\eta \neq 0$, and the right-hand that for $\eta = 0$.

Generalising this result to all β as described above, we obtain

$$F_{lm}(\eta) = -\frac{2-\beta}{2+\beta}\left(\left|\frac{2+2\gamma-\beta\gamma}{\beta\tilde{U}^2+\beta-2}\right| - \frac{\gamma m}{l\tilde{\kappa}+m\tilde{\Omega}}\right)\frac{ie^{-i\hat{\eta}\ln\frac{l\tilde{\kappa}+m\tilde{\Omega}}{\tilde{\omega}}}}{(1-e^{2\pi\hat{\eta}})}, \qquad \eta \neq 0. \tag{C9}$$

This expression is singular when $\eta = 0$. As we now demonstrate, $F_{lm}(\eta)$ contains a delta-function at $\eta = 0$. For the case $\Omega_{\rm p} = 0$, $s = 0$, we can integrate the expression for $F_{lm}(\eta)$ directly:

$$J_1(0,\eta) = \frac{1}{l\tilde{\kappa}+m\tilde{\Omega}}\frac{1}{2\pi}\int_{-\infty}^{\infty} e^{-i\eta h}dh = \frac{1}{l\tilde{\kappa}+m\tilde{\Omega}}\delta(\eta). \tag{C10}$$

and so for the general power-law disk

$$F_{lm}(\eta) = \frac{2-\beta}{2+\beta}\left\{\left|\frac{2+2\gamma-\beta\gamma}{\beta\tilde{U}^2+\beta-2}\right| - \frac{\gamma m}{l\tilde{\kappa}+m\tilde{\Omega}}\right\}\delta(\hat{\eta}). \tag{C11}$$

To obtain the expression for general $\Omega_{\rm p}$ and s, we write

$$J_1(0,\eta) = J_1^{(1)}(0,\eta) + J_1^{(2)}\delta(\eta), \tag{C12}$$

where $J_1^{(1)}(0,\eta)$ is equal to our previous expression (C8) for $J_1(0,\eta)$. We integrate (C12) over η, thus smoothing out the delta-function.

$$\int_{\eta=-\epsilon}^{+\epsilon} d\eta\, J_1(0,\eta) = \int_{\eta=-\epsilon}^{+\epsilon} d\eta\, J_1^{(1)}(0,\eta) + J_1^{(2)}\int_{\eta=-\epsilon}^{+\epsilon} d\eta\,\delta(\eta), \tag{C13}$$

We now let $\epsilon \to 0$. We see from the expression for $J_1^{(1)}(\eta)$ already obtained (C8) that $J_1^{(1)}(\eta)$ is odd in the limit of vanishingly small η. It therefore contributes nothing in (C13). Using the expression (C3) for $J_1(0,\eta)$, we obtain

$$J_1^{(2)} = \lim_{\epsilon\to 0}\frac{1}{2\pi}\int_{\eta=-\epsilon}^{+\epsilon} d\eta \int_{h=-\infty}^{\infty} dh \frac{e^{-i\eta h}}{l\tilde{\kappa}+m\tilde{\Omega}-\tilde{\omega}e^h} \tag{C14}$$

Swapping the order of integration and performing the integration over η, we obtain

$$J_1^{(2)} = \lim_{\epsilon\to 0}\frac{1}{2\pi i}\int_{h=-\infty}^{\infty} \frac{dh}{h}\frac{e^{i\epsilon h}-e^{-i\epsilon h}}{l\tilde{\kappa}+m\tilde{\Omega}-\tilde{\omega}e^h} \tag{C15}$$

We evaluate this by carrying out two separate contour integrals. For the integral with $e^{-i\epsilon h}$, we close the contour in the lower half-plane, as shown in the left-hand plot of fig. C1. As usual, we take the radius of the inner semi-circle to zero, and the that of the outer semi-circle to infinity. The integrand then vanishes on the outer semi-circle, and we obtain

$$\frac{1}{2\pi i}\int_{h=-\infty}^{\infty} \frac{dh}{h}\frac{e^{-i\epsilon h}}{l\tilde{\kappa}+m\tilde{\Omega}-\tilde{\omega}e^h} = \frac{1}{l\tilde{\kappa}+m\tilde{\Omega}}\sum_{n=-1}^{-\infty}\frac{e^{-i\epsilon\ln\frac{l\tilde{\kappa}+m\tilde{\Omega}}{\tilde{\omega}}}e^{2n\pi\epsilon}}{\ln\frac{l\tilde{\kappa}+m\tilde{\Omega}}{\tilde{\omega}}+2in\pi} - \frac{1}{2}\frac{1}{l\tilde{\kappa}+m\tilde{\Omega}-\tilde{\omega}} \tag{C16}$$

The integral with $e^{+i\epsilon h}$ is evaluated over an analogous contour in the upper half-plane. We obtain

$$\frac{1}{2\pi i}\int_{h=-\infty}^{\infty}\frac{dh}{h}\frac{e^{i\epsilon h}}{l\tilde{\kappa}+m\tilde{\Omega}-\tilde{\omega}e^{h}}=-\frac{1}{l\tilde{\kappa}+m\tilde{\Omega}}\sum_{n=0}^{\infty}\frac{e^{i\epsilon\ln\frac{l\tilde{\kappa}+m\tilde{\Omega}}{\tilde{\omega}}}e^{-2n\pi\epsilon}}{\ln\frac{l\tilde{\kappa}+m\tilde{\Omega}}{\tilde{\omega}}+2in\pi}+\frac{1}{2}\frac{1}{l\tilde{\kappa}+m\tilde{\Omega}-\tilde{\omega}} \tag{C17}$$

Subtracting these two results and taking the limit $\epsilon\to 0$, we obtain

$$\frac{1}{2\pi i}\int_{h=-\infty}^{\infty}\frac{dh}{h}\frac{e^{i\epsilon h}-e^{-i\epsilon h}}{l\tilde{\kappa}+m\tilde{\Omega}-\tilde{\omega}e^{h}}=\frac{1}{l\tilde{\kappa}+m\tilde{\Omega}-\tilde{\omega}}+\frac{i}{l\tilde{\kappa}+m\tilde{\Omega}}\sum_{n=-\infty}^{\infty}\frac{1}{2n\pi-i\ln\frac{l\tilde{\kappa}+m\tilde{\Omega}}{\tilde{\omega}}} \tag{C18}$$

The sum can be explicitly evaluated.

$$\begin{aligned}\sum_{n=-\infty}^{\infty}\frac{1}{2n\pi-iz}&=-\frac{1}{iz}+\sum_{n=-1}^{-\infty}\frac{1}{2n\pi-iz}+\sum_{n=1}^{\infty}\frac{1}{2n\pi-iz}=\frac{i}{z}+2iz\sum_{n=1}^{\infty}\frac{1}{(2n\pi)^2+z^2}\\&=\frac{iz}{4\pi^2}\sum_{n=-\infty}^{\infty}\frac{1}{(n+iz/2\pi)(n-iz/2\pi)}=-\frac{1}{2}\cot\frac{iz}{2}=-\frac{i}{2}\frac{e^{-z}+1}{e^{-z}-1}\end{aligned} \tag{C19}$$

where we have used the standard result (Prudnikov *et al.* 1986, eq. (5.1.6.4))

$$\sum_{n=-\infty}^{\infty}\frac{1}{(n+a)(n+b)}=\frac{\pi}{b-a}(\cot\pi a-\cot\pi b) \tag{C20}$$

Thus we obtain

$$J_1^{(2)}=\frac{1}{2(l\tilde{\kappa}+m\tilde{\Omega})} \tag{C21}$$

The angular momentum function for the self-consistent disk is then

$$F_{lm}(\eta)=\frac{2-\beta}{2+\beta}\left(\left|\frac{2+2\gamma-\beta\gamma}{\beta\tilde{U}^2+\beta-2}\right|-\frac{\gamma m}{l\tilde{\kappa}+m\tilde{\Omega}}\right)\left(\frac{1}{2}\delta(\hat{\eta})-\frac{ie^{-i\hat{\eta}\ln\frac{l\tilde{\kappa}+m\tilde{\Omega}}{\tilde{\omega}}}}{1-e^{2\pi\hat{\eta}}}\right). \tag{C22}$$

The corresponding result for the Toomre-Zang disk is (correcting a typographical error in Zang (1976), eq. (Z3.43))

$$F_{lm}(\eta)=\left(\gamma+1-\frac{\gamma m}{l\tilde{\kappa}+m\tilde{\Omega}}\right)\left(\frac{1}{2}\delta(\eta)-\frac{ie^{-i\eta\ln\frac{l\tilde{\kappa}+m\tilde{\Omega}}{\tilde{\omega}}}}{1-e^{2\pi\eta}}\right). \tag{C23}$$

C2 The inner cut-out disk

Here, we must evaluate

$$J_1(0,\eta)=\frac{1}{2\pi}\int_{-\infty}^{\infty}\frac{e^{-i\eta h}}{l\tilde{\kappa}+m\tilde{\Omega}-\tilde{\omega}e^{h}}\frac{e^{Nh}}{e^{Nh}+1}dh,\qquad J_2(0,\eta)=\frac{1}{2\pi}\int_{-\infty}^{\infty}\frac{e^{-i\eta h}}{l\tilde{\kappa}+m\tilde{\Omega}-\tilde{\omega}e^{h}}\frac{Ne^{Nh}}{(e^{Nh}+1)^2}dh. \tag{C24}$$

Again the integrands have poles when $h=\ln[(l\tilde{\kappa}+m\tilde{\Omega})/\tilde{\omega}]+2ni\pi$. However, they now also have poles along the imaginary axis, at $h_j=(2j-1)i\pi/N$, where j is an integer. We integrate around the same rectangular contour as for the self-consistent disk (fig. C1). As well as the pole at $\ln[(l\tilde{\kappa}+m\tilde{\Omega})/\tilde{\omega}]$, we now also enclose N poles lying on the imaginary axis. Adding up the residues from all these poles, we obtain the result:

$$J_1(0,\eta)=\frac{-i}{1-e^{2\pi\eta}}\left\{\frac{(l\tilde{\kappa}+m\tilde{\Omega})^{N-1}e^{-i\eta\ln\frac{l\tilde{\kappa}+m\tilde{\Omega}}{\tilde{\omega}}}}{(l\tilde{\kappa}+m\tilde{\Omega})^N+\tilde{\omega}^N}-\frac{1}{N}\sum_{j=1}^{N}\frac{e^{\frac{2j-1}{N}\pi\eta}}{l\tilde{\kappa}+m\tilde{\Omega}-\tilde{\omega}e^{\frac{2j-1}{N}i\pi}}\right\}, \tag{C25}$$

$$\begin{aligned}J_2(0,\eta)=-\frac{i}{1-e^{2\pi\eta}}\times\Bigg\{&\frac{(l\tilde{\kappa}+m\tilde{\Omega})^{N-1}N\tilde{\omega}^Ne^{-i\eta\ln\frac{l\tilde{\kappa}+m\tilde{\Omega}}{\tilde{\omega}}}}{\left[(l\tilde{\kappa}+m\tilde{\Omega})^N+\tilde{\omega}^N\right]^2}\\&+\frac{1}{N}\sum_{j=1}^{N}\frac{e^{\frac{2j-1}{N}\pi\eta}}{l\tilde{\kappa}+m\tilde{\Omega}-\tilde{\omega}e^{\frac{2j-1}{N}i\pi}}\left[i\eta-\frac{\tilde{\omega}e^{\frac{2j-1}{N}i\pi}}{l\tilde{\kappa}+m\tilde{\Omega}-\tilde{\omega}e^{\frac{2j-1}{N}i\pi}}\right]\Bigg\}.\end{aligned} \tag{C26}$$

For $\beta \neq 0$, we obtain the angular momentum function

$$F_{lm}(\eta \neq 0) = -\frac{i}{1-e^{2\pi\hat{\eta}}} \times \left\{ \frac{(l\tilde{\kappa}+m\tilde{\Omega})^{N-1} e^{-i\hat{\eta}\ln\frac{l\tilde{\kappa}+m\tilde{\Omega}}{\tilde{\omega}}}}{(l\tilde{\kappa}+m\tilde{\Omega})^N+\tilde{\omega}^N} \right.$$
$$\times \left[\frac{2-\beta}{2+\beta} \left((l\tilde{\kappa}+m\tilde{\Omega}) \left| \frac{2+2\gamma-\beta\gamma}{\beta\tilde{U}^2+\beta-2} \right| - \gamma m \right) - \frac{mN\tilde{\omega}^N}{(l\tilde{\kappa}+m\tilde{\Omega})^N+\tilde{\omega}^N} \right]$$
$$\left. - \frac{1}{N}\sum_{j=1}^{N} \frac{e^{\frac{2j-1}{N}\pi\hat{\eta}}}{l\tilde{\kappa}+m\tilde{\Omega}-\tilde{\omega}e^{\frac{2j-1}{N}i\pi}} \left[\frac{m\tilde{\omega}e^{\frac{2j-1}{N}i\pi}}{l\tilde{\kappa}+m\tilde{\Omega}-\tilde{\omega}e^{\frac{2j-1}{N}i\pi}} - im\hat{\eta} + \frac{2-\beta}{2+\beta}\left((l\tilde{\kappa}+m\tilde{\Omega}) \left| \frac{2+2\gamma-\beta\gamma}{\beta\tilde{U}^2+\beta-2} \right| - \gamma m \right) \right] \right\}. \tag{C27}$$

We can use l'Hôpital's rule to obtain the result for $\eta = 0$. This requires that both the numerator and denominator of (C27) are zero in the limit $\eta \to 0$. The denominator $(1-e^{2\pi\eta})$ is obviously zero in this limit, and it can be shown that the numerator is also (e.g. it is readily apparent for $N = 1$). Application of l'Hôpital's rule then yields

$$F_{lm}(\eta = 0) = -\frac{i}{2\pi} \left\{ \frac{i(l\tilde{\kappa}+m\tilde{\Omega})^{N-1}\ln\frac{l\tilde{\kappa}+m\tilde{\Omega}}{\tilde{\omega}}}{(l\tilde{\kappa}+m\tilde{\Omega})^N+\tilde{\omega}^N} \left[\frac{2-\beta}{2+\beta} \left((l\tilde{\kappa}+m\tilde{\Omega}) \left| \frac{2+2\gamma-\beta\gamma}{\beta\tilde{U}^2+\beta-2} \right| - \gamma m \right) - \frac{mN\tilde{\omega}^N}{(l\tilde{\kappa}+m\tilde{\Omega})^N+\tilde{\omega}^N} \right] \right.$$
$$+ \frac{1}{N}\sum_{j=1}^{N} \frac{1}{l\tilde{\kappa}+m\tilde{\Omega}-\tilde{\omega}e^{\frac{2j-1}{N}i\pi}}$$
$$\left. \times \left((2j-1)\frac{\pi}{N} \left[\frac{m\tilde{\omega}e^{\frac{2j-1}{N}i\pi}}{l\tilde{\kappa}+m\tilde{\Omega}-\tilde{\omega}e^{\frac{2j-1}{N}i\pi}} + \frac{2-\beta}{2+\beta}\left((l\tilde{\kappa}+m\tilde{\Omega}) \left| \frac{2+2\gamma-\beta\gamma}{\beta\tilde{U}^2+\beta-2} \right| - \gamma m \right) \right] - im \right) \right\}. \tag{C28}$$

C3 The doubly cut-out disk

We briefly summarise the results for the doubly cut-out disks. Here,

$$J_1(0,\eta,\tilde{L}_c) = \frac{1}{2\pi}\int_{-\infty}^{\infty} \frac{e^{-i\eta h}}{l\tilde{\kappa}+m\tilde{\Omega}-\tilde{\omega}e^h} \frac{e^{Nh}}{\left[e^{Nh}+1\right]\left[\tilde{L}_c^{-M_\beta}e^{Mh}+1\right]}dh, \tag{C29}$$

$$J_2(0,\eta,\tilde{L}_c) = \frac{1}{2\pi}\int_{-\infty}^{\infty} \frac{e^{-i\eta h}}{l\tilde{\kappa}+m\tilde{\Omega}-\tilde{\omega}e^h} \frac{Ne^{Nh}\left(\tilde{L}_c^{-M_\beta}e^{Mh}+1\right) - M\tilde{L}_c^{-M_\beta}e^{Nh}e^{Mh}}{\left[e^{Nh}+1\right]^2\left[\tilde{L}_c^{-M_\beta}e^{Mh}+1\right]^2}dh. \tag{C30}$$

The integrand now has additional poles at $h_k = (2k-1)i\pi/M + (2+\beta)/(2-\beta) \times \ln\tilde{L}_c$, where k is an integer. We thus obtain a second sum, and F_{lm} becomes

$$F_{lm}(\eta \neq 0) = \frac{-i}{1-e^{2\pi\hat{\eta}}} \times \left\{ \frac{(l\tilde{\kappa}+m\tilde{\Omega})^{N-1}\tilde{L}_c^{M_\beta}\tilde{\omega}^M e^{-i\hat{\eta}\ln\frac{l\tilde{\kappa}+m\tilde{\Omega}}{\tilde{\omega}}}}{\left[(l\tilde{\kappa}+m\tilde{\Omega})^N+\tilde{\omega}^N\right]\left[(l\tilde{\kappa}+m\tilde{\Omega})^M+\tilde{L}_c^{M_\beta}\tilde{\omega}^M\right]} \right.$$
$$\times \left[\frac{2-\beta}{2+\beta}\left((l\tilde{\kappa}+m\tilde{\Omega}) \left| \frac{2+2\gamma-\beta\gamma}{\beta\tilde{U}^2+\beta-2} \right| - \gamma m \right) - \frac{mN\tilde{\omega}^N}{(l\tilde{\kappa}+m\tilde{\Omega})^N+\tilde{\omega}^N} + \frac{mM(l\tilde{\kappa}+m\tilde{\Omega})^M}{(l\tilde{\kappa}+m\tilde{\Omega})^M+\tilde{L}_c^{M_\beta}\tilde{\omega}^M} \right]$$
$$- \frac{\tilde{L}_c^{M_\beta}}{N}\sum_{j=1}^{N} \frac{e^{\frac{2j-1}{N}\pi\hat{\eta}}}{\left[e^{(2j-1)\frac{M}{N}i\pi}+\tilde{L}_c^{M_\beta}\right]\left[l\tilde{\kappa}+m\tilde{\Omega}-\tilde{\omega}e^{\frac{2j-1}{N}i\pi}\right]}$$
$$\times \left[\frac{m\tilde{\omega}e^{\frac{2j-1}{N}i\pi}}{l\tilde{\kappa}+m\tilde{\Omega}-\tilde{\omega}e^{\frac{2j-1}{N}i\pi}} - im\hat{\eta} + \frac{2-\beta}{2+\beta}\left((l\tilde{\kappa}+m\tilde{\Omega}) \left| \frac{2+2\gamma-\beta\gamma}{\beta\tilde{U}^2+\beta-2} \right| - \gamma m \right) \right] \tag{C31}$$
$$+ \frac{\tilde{L}_c^{N_\beta}}{M}e^{-i\hat{\eta}\frac{2+\beta}{2-\beta}\ln\tilde{L}_c}\sum_{k=1}^{M} \frac{e^{\frac{2k-1}{M}\pi\hat{\eta}}}{\left[e^{-(2k-1)\frac{N}{M}i\pi}+\tilde{L}_c^{N_\beta}\right]\left[l\tilde{\kappa}+m\tilde{\Omega}-\tilde{\omega}\tilde{L}_c^{\frac{2+\beta}{2-\beta}}e^{\frac{2k-1}{M}i\pi}\right]}$$
$$\left. \times \left[\frac{m\tilde{\omega}\tilde{L}_c^{\frac{2+\beta}{2-\beta}}e^{\frac{2k-1}{M}i\pi}}{l\tilde{\kappa}+m\tilde{\Omega}-\tilde{\omega}\tilde{L}_c^{\frac{2+\beta}{2-\beta}}e^{\frac{2k-1}{M}i\pi}} - im\hat{\eta} + \frac{2-\beta}{2+\beta}\left((l\tilde{\kappa}+m\tilde{\Omega}) \left| \frac{2+2\gamma-\beta\gamma}{\beta\tilde{U}^2+\beta-2} \right| - \gamma m \right) \right] \right\}.$$

In the limit $\eta \to 0$:

$$
\begin{aligned}
F_{lm}(\eta=0) = -\frac{i}{2\pi} \times \Bigg\{ & \frac{i(l\tilde{\kappa}+m\tilde{\Omega})^{N-1}\tilde{L}_c^{M_\beta}\tilde{\omega}^M \ln\frac{l\tilde{\kappa}+m\tilde{\Omega}}{\tilde{\omega}}}{\left[(l\tilde{\kappa}+m\tilde{\Omega})^N+\tilde{\omega}^N\right]\left[(l\tilde{\kappa}+m\tilde{\Omega})^M+\tilde{L}_c^{M_\beta}\tilde{\omega}^M\right]} \\
& \times \left[\frac{2-\beta}{2+\beta}\left((l\tilde{\kappa}+m\tilde{\Omega})\left|\frac{2+2\gamma-\beta\gamma}{\beta\tilde{U}^2+\beta-2}\right|-\gamma m\right)-\frac{mN\tilde{\omega}^N}{(l\tilde{\kappa}+m\tilde{\Omega})^N+\tilde{\omega}^N}+\frac{mM(l\tilde{\kappa}+m\tilde{\Omega})^M}{(l\tilde{\kappa}+m\tilde{\Omega})^M+\tilde{L}_c^{M_\beta}\tilde{\omega}^M}\right] \\
& + \frac{\tilde{L}_c^{M_\beta}}{N}\sum_{j=1}^{N}\frac{1}{\left[e^{(2j-1)\frac{M}{N}i\pi}+\tilde{L}_c^{M_\beta}\right]\left[l\tilde{\kappa}+m\tilde{\Omega}-\tilde{\omega}e^{\frac{2j-1}{N}i\pi}\right]} \\
& \times \left[(2j-1)\frac{\pi}{N}\left\{\frac{m\tilde{\omega}e^{\frac{2j-1}{N}i\pi}}{\left[l\tilde{\kappa}+m\tilde{\Omega}-\tilde{\omega}e^{\frac{2j-1}{N}i\pi}\right]}+\frac{2-\beta}{2+\beta}\left((l\tilde{\kappa}+m\tilde{\Omega})\left|\frac{2+2\gamma-\beta\gamma}{\beta\tilde{U}^2+\beta-2}\right|-\gamma m\right)\right\}-im\right] \qquad \text{(C32)} \\
& - \frac{\tilde{L}_c^{N_\beta}}{M}\sum_{k=1}^{M}\frac{1}{\left[e^{-(2k-1)\frac{N}{M}i\pi}+\tilde{L}_c^{N_\beta}\right]\left[l\tilde{\kappa}+m\tilde{\Omega}-\tilde{\omega}\tilde{L}_c^{\frac{2+\beta}{2-\beta}}e^{\frac{2k-1}{M}i\pi}\right]} \\
\times & \left[\left\{\frac{(2k-1)\pi}{M}-i\ln\tilde{L}_c^{\frac{2+\beta}{2-\beta}}\right\}\left\{\frac{m\tilde{\omega}\tilde{L}_c^{\frac{2+\beta}{2-\beta}}e^{\frac{2k-1}{M}i\pi}}{l\tilde{\kappa}+m\tilde{\Omega}-\tilde{\omega}\tilde{L}_c^{\frac{2+\beta}{2-\beta}}e^{\frac{2k-1}{M}i\pi}}+\frac{2-\beta}{2+\beta}\left((l\tilde{\kappa}+m\tilde{\Omega})\left|\frac{2+2\gamma-\beta\gamma}{\beta\tilde{U}^2+\beta-2}\right|-\gamma m\right)\right\}-im\right]\Bigg\}.
\end{aligned}
$$